Patterning porous networks through self-assembly of programmed biomacromolecules

Laure-Elie Carloni,[†] C. Grazia Bezzu[†] and Davide Bonifazi*

[a] Dr. L.-E. Carloni, Department of Chemistry and Namur Research College (NARC), University of Namur, Rue de Bruxelles 61, Namur, 5000, Belgium.

[b] Dr. C. G. Bezzu, Prof. Dr. D. Bonifazi

Cardiff University, School of Chemistry, Park Place, Main Building, CF10 3AT, Cardiff, Wales, UK.

Email: bonifazid@cardiff.ac.uk

† These authors equally contributed to this work.

[ ] D.B. and C.G.B. gratefully acknowledges the EU through the MSCA-RISE (project INFUSION) funding scheme and Cardiff University for generous financial support. L.-E.C. gratefully acknowledges the FRS-FNRS for her doctoral FRIA fellowship.

Keywords: porous materials, 2D self-assembly, self-organisation, DNA nanotechnology, proteins, peptides, surfaces, scanning probe microscopy, host-guest, supramolecular chemistry

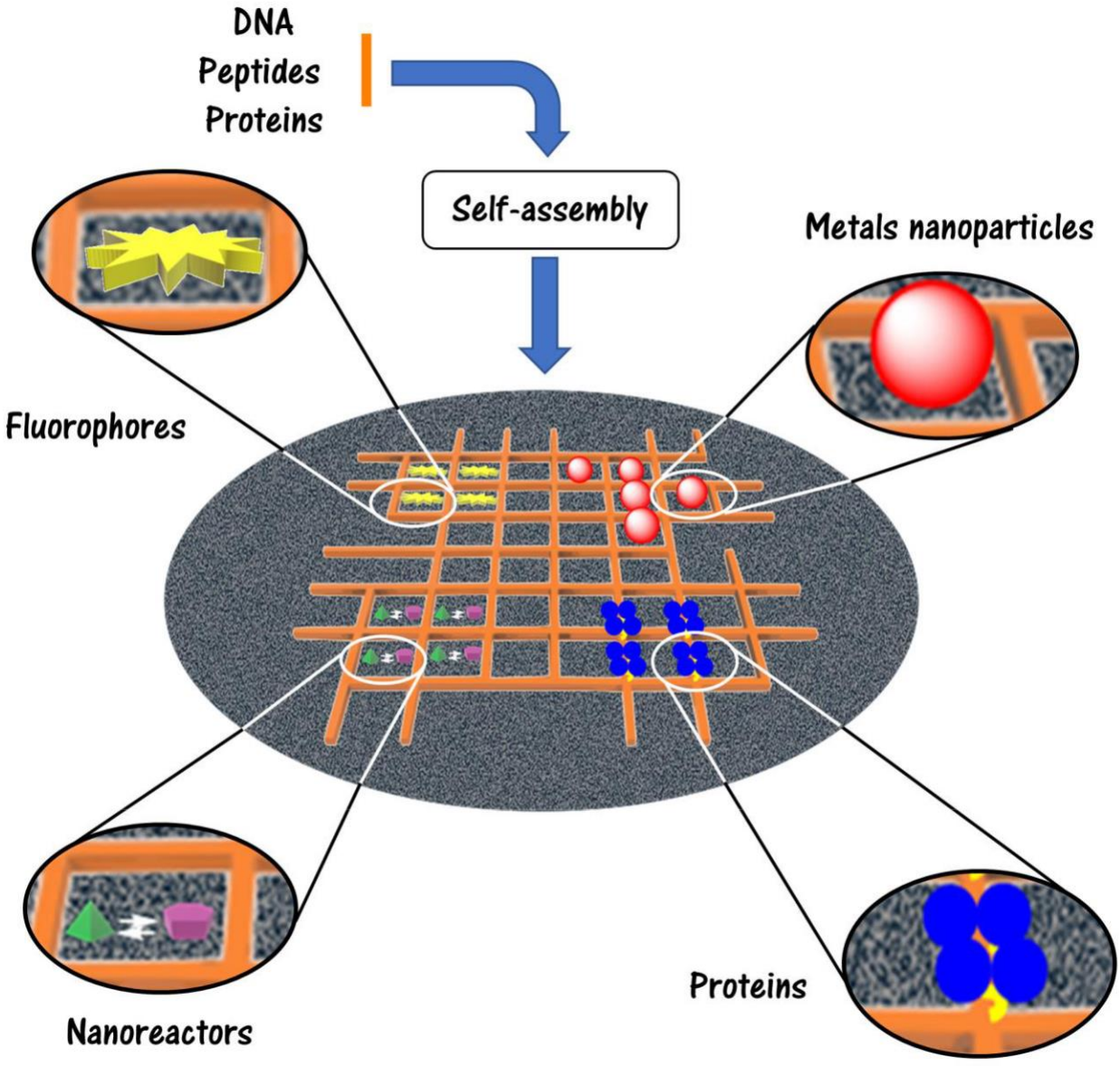

3, 2, 1, assemble! Patterning surfaces with extended porous networks represents a viable method for the fabrication of multifunctional materials with potential applications in nanotechnology, nanoelectronics, sensing and catalysis. These networks can indeed serve as templates for hosting or anchoring guests, such as nanoparticles, proteins and fluorophores, thus leading to regularly spaced arrays. This review provides an overview on the current bottom-up approaches

towards the engineering of porous nanostructures using nucleic acids, peptides and proteins scaffolds.

Laure-Elie Carloni obtained her PhD in chemistry in 2015 from the University of Namur (Belgium) under the supervision of Prof. Dr. Davide Bonifazi. Her doctoral work focused on the synthesis of peptide nucleic acids and peptides, peculiarly functionalized for supramolecular self-assembly purposes. Thereafter, she joined the Janssen Pharmaceutical Companies of Johnson & Johnson, first as a postdoctoral fellow, then as a permanent scientist, in the Analytical R&D department.

C. Grazia Bezzu obtained her PhD in Chemistry in 2009 from Cardiff University under the supervision of Prof. Neil McKeown. Her doctoral project was based on the preparation of Nanoporous Molecular Crystals from novel Phthalocyanine derivatives. Thereafter, she worked as a Post-Doctoral Researcher in the McKeown group, where she investigated novel microporous organic materials. In March 2018, she joined the research group of Prof. Davide Bonifazi at Cardiff University, where she works on the preparation and supramolecular assembly of chalcogen containing aromatic molecules.

Davide Bonifazi was born in Guastalla (Italy) in 1975. After obtaining the "Laurea" in "Industrial Chemistry" from the University of Parma working with Prof. Enrico Dalcanale, he joined the group of Prof. François Diederich as PhD student at the ETH Zürich (2000-2004). He was awarded the Silver Medallion of the ETH for his doctoral dissertation (2005). After a one-year postdoctoral fellowship with Prof. Maurizio Prato at University of Trieste, he joined the same

University as a research associate first, and then as a part-time Professor (2012-2015). In 2006, he joined the University of Namur (BE) as Junior Professor (2006-2011) and as Professor of Organic Chemistry (2012-2015). Since 2016 he is Chair Professor of Organic Supramolecular Chemistry in the School of Chemistry at Cardiff University (UK). His activities are focused on the creation of functional organic architectures in interdisciplinary projects through targeted organic synthesis, self-assembly, and self-organization of organic architectures in solution and on surfaces, physical-organic studies, material- and bio-based design.

Abstract: Two-dimensional porous networks are of great interest for the fabrication of complex organised functional materials for potential applications in nanotechnologies and nanoelectronics. This review aims at providing an overview of bottom-up approaches towards the engineering of two-dimensional porous networks using biomacromolecules, with a particular focus on nucleic acids and proteins. The first part illustrates how the advancements in DNA nanotechnology allowed the attainment of complex ordered porous two-dimensional DNA nanostructures, thanks to a biomimetic approach based on DNA molecules self-assembly via specific hydrogen-bond base-pairing. The second part focuses the attention on how polypeptides and proteins structural properties could be used to engineer organised networks templating the formation of multifunctional materials. The structural organisation of all examples is discussed as revealed by scanning probe microscopy or transmission electron microscopy imaging techniques.

Figure for the Table of Content

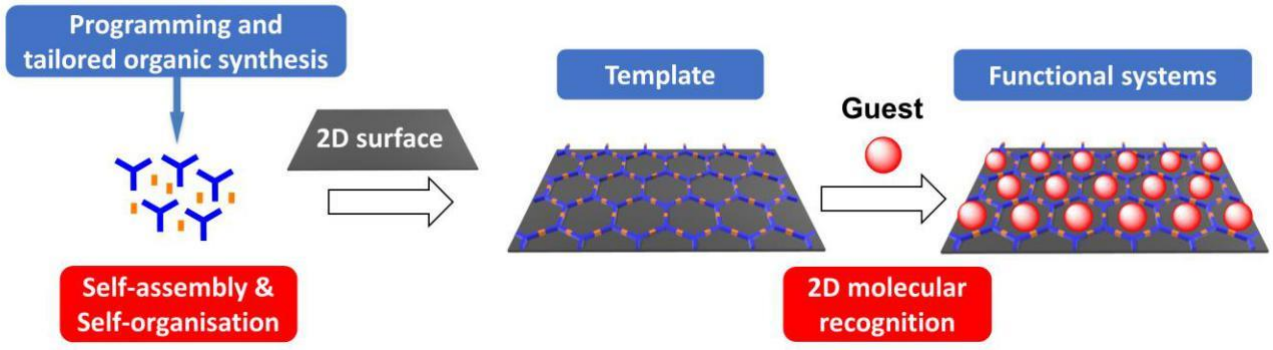

Introduction.

Surfaces patterned with two-dimensional porous networks are particularly interesting nanostructures as their cavities can be used to host remotely controlled organic molecules (*e.g.* molecular switches, luminescent chromophores), bringing functionality, structural organisation and device-like features to the material at the nanoscale level. For example, the colour quality and the intensity of the emission signal of organic and metal-complex luminophores in electroluminescent devices are dramatically altered due to their susceptibility to the structural organisation at the molecular level (*e.g.* their tendency to aggregate in solution), which induces interchromophoric interactions.[1] Therefore, their surface confinement could enhance their emissive properties.[2] Porous networks on surfaces may not only serve as templates for the precise localisation of species, but also, if properly equipped, as nanoreactors for the chemical transformation of encapsulated molecular reagents exploiting the spatial confinement as

a strategy to achieve control over the chemical reactivity, as shown in 3D structures.[3] 2D porous networks can also be used to stabilise reactive species by isolating guests from the bulk environment or to catalyse reactions effectively due to guest discrimination.[2a, 4] In addition, they can be employed as nanostructure templates for polymers stamps for soft lithography applications.[5] Furthermore, unlike the investigation in solutions and crystals, working on surfaces allows the direct addressing of the molecular components on a nanometric scale (~1-100 nm), affording the best integration of the system into usable macroscopic devices. Therefore, the best engineering methodology involves modifying the surfaces of bulk materials such as metals or semiconductors by deposition of functional organic materials that undergoing programmed[6] self-assembly[7] give rise to the formation of porous architecture of defined structural properties. The invention of scanning probe microscopies (*e.g.* scanning tunnelling microscopy (STM) and atomic force microscopy (AFM))[8] enabled the nanoscale investigation of these two-dimensional architectures in direct space, hence facilitating the characterisation of the architectures and, thus, the tailoring of materials properties.

Although the construction of two-dimensional nanoporous patterned surfaces using surface-confined covalent reactions or preformed covalent macrocycles can be quite successful and lead to stable architectures,[2a, 9] however their generally complex product distribution and synthetic reproducibility on a surface constitutes an

important limitation of this approach. In addition, the introduction of desired modifications of the size and shape of the resulting cavities is not straightforward. A promising alternative strategy to selectively and spontaneously form ordered porous domains on surfaces is the hierarchical self-assembly of small molecules.[10] The main approaches used for the formation of these systems consist of multiple non-covalent interactions (namely H-bonding[11], metal-ligand,[12] dipole-dipole,[13] van der Waals interactions[11p, 14] and σ-hole interactions[15]) established between precursor molecular modules.[2a, 9, 15d, 16] The latter are designed with defined recognition sites, which dictate their non-covalent auto-organisation, leading to the formation of the desired two-dimensional arrays. Hence, the arrangement of the assemblies is solely directed by the information embedded within programmed molecular modules. This supramolecular approach offers considerable advantages over any other methodologies (*i.e.* "top-down" or covalent) for the construction of ordered structures with nanometre precision over an extended large scale. Indeed, *(i)* the equilibrium between the constituents and the final product, along with *(ii)* the dynamicity of the chemical systems toward multi-stable nanostructured materials, contribute to the self-rearrangement of the components within the assembled structure and thus to the controlled positioning of molecules.[17] Building on this approach, spectacular porous architectures featuring different structural properties and shapes have been developed so far, and the interested reader is directed to specific

reviews on the topic.[2a, 9, 15d, 16]

Inspired by the small molecule approach, the field has recently expanded toward the development of porous structures using programmed, water-soluble biological macromolecules as self-assembly building blocks (Figure 1).

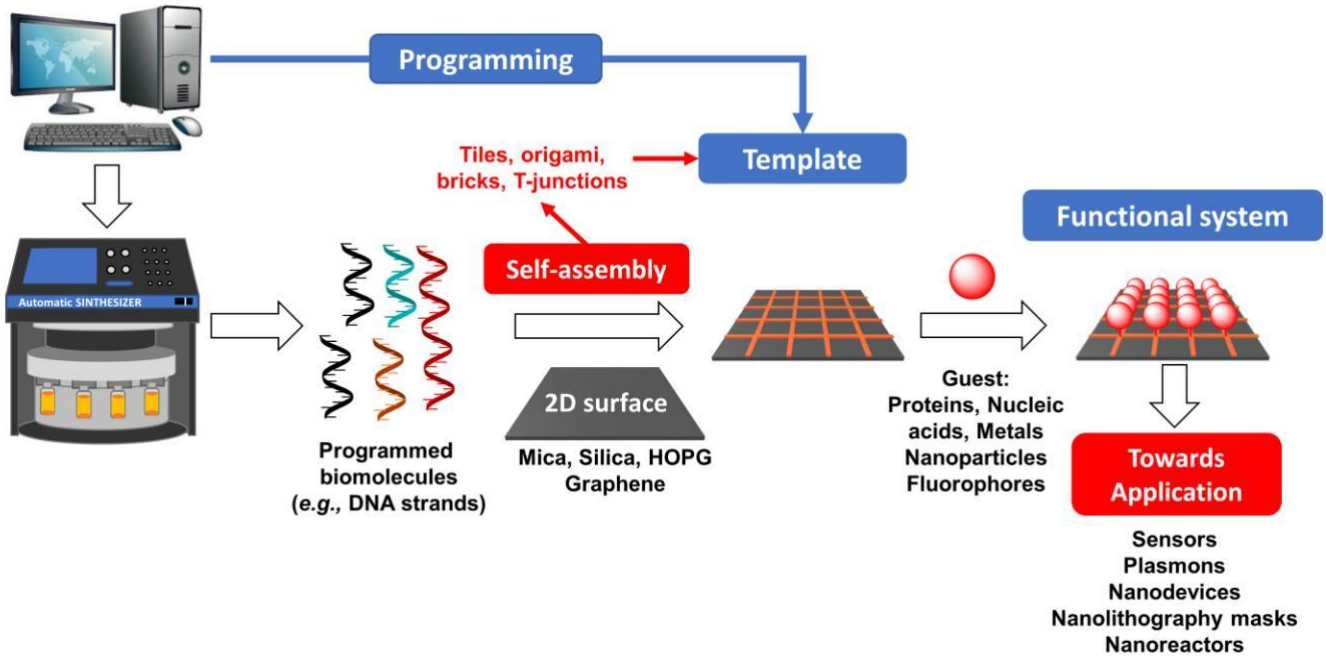

Figure 1. Programming 2D porous networks with biomacromolecules.

With such systems, tailored patterned surfaces are prepared directly from aqueous solutions containing the relevant biomacromolecule through spin casting under ambient conditions. This approach avoids the use of thermal evaporators and expensive high-vacuum systems, which are typically used for small molecules. Amongst the possible biological macromolecules, nucleic acids and peptides/proteins certainly represent

the most appealing architectures as one can tailor their self-assembly properties through specific sequencing of their nucleobase and amino acid constituents, respectively.

For instance, building on the unique recognition ability of deoxyribonucleic acid (DNA) and fascinating developments of DNA nanotechnology,[18] extended and porous arrays featuring different pore sizes could be accurately formed. Similarly, porous functional nanostructures and patterns could be formed on surfaces with structurally tailored peptides and proteins.[19] Considering that those biomacromolecules are nowadays easily accessible through automized synthetic protocols, these porous macromolecular systems are at the forefront of nanotechnology. It is for these reasons, that in this review we aim to give an overview on the most recent developments on porous 2D materials on surfaces. The manuscript is organised in three chapters, the first dealing with networks constructed with nucleic acids, the second describing peptide and protein-based arrays and the third focused on role of the surface in the assembly.

Porous networks through self-assembly of DNA macromolecules.

The main strategy to form functional two-dimensional nanostructures on surfaces based on DNA consists of the directed hybridisation of DNA tiles.[18a, 20] DNA tiles (**A**, **B**, Figure 2) are specific *N*-armed junction DNA constructs composed of individual DNA units, bearing "sticky" ends.[21] The latter are protrusions of short single DNA strands, which

allow the specific inter-hybridisation of the DNA tiles, and thus their self-assembly into the desired nanostructures (**C**, Figure 2).

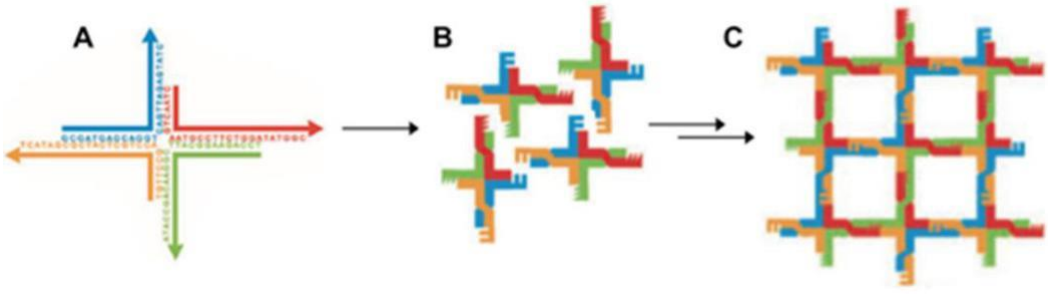

Figure 2. Schematic illustration of DNA tiles. Diagram A shows the *N*-armed junction DNA constructs composed of individual DNA units, bearing "sticky" ends. This particular example shows a square planar *4*-armed junction. Four oligonucleotides hybridise with two pairs of complementary "sticky" ends. Diagram B illustrates the square planar junctions, highlighting the positions of complementary sticky ends (red sticky ends are complementary to green sticky ends; orange sticky ends are complementary to blue sticky ends). Diagram C displays the resulting square lattice that should be formed from the self-assembly of the *4*-armed junctions. The oligonucleotides are shown as simplified backbone traces.[22] Adapted from ref [22] with permission from WILEY‐VCH Verlag GmbH & Co. KGaA, Weinheim, Copyright 2005

The first DNA tile, the immobile four-way junction built from 4 single strand DNA, was reported by Seeman and co-workers in 1983.[23] This lacked the necessary rigidity for the formation of extended periodic arrays.[24] In the same manner others subsequently formed junctions of this kind with 3, 5, 6, 8 and 12 arms.[24a, 25] The rigidity as well as the second dimension of the resulting nanostructures are governed by the design of the *N*-armed junctions. The core of DNA tiles can mainly be constructed *via* two similar strategies. The first one is based on DNA double-crossover (DX) motifs **1**, *i.e.* small tiles (ca. 4 16 nm^2) which contain two parallel double helices held together by two crossovers (Figure 3). In order to impart greater rigidity to the

resulting nanostructures, more complex motifs were derived from the DX basic design.[18a, f, 20b-d, 26] For instance, DX junction **2** can be constructed using five strands, where three of them are involved in the crossovers, while the two others are fixed to a given helical domain. One of the strands is circular and complementary to those fixed in the central portion (Figure 3).[20b] Another example consists of DNA triple-crossover (TX) motifs **3**, which can be prepared using three distinct helices instead of two, and thus with twice the number of crossovers (Figure 3).[27] The second strategy is based on DNA origami. DNA origami motifs **4** (Figure 3), conceived by Rothemund in 2006,[28] consist of a viral DNA strand folded into desired two-dimensional or tri-dimensional nanostructures.

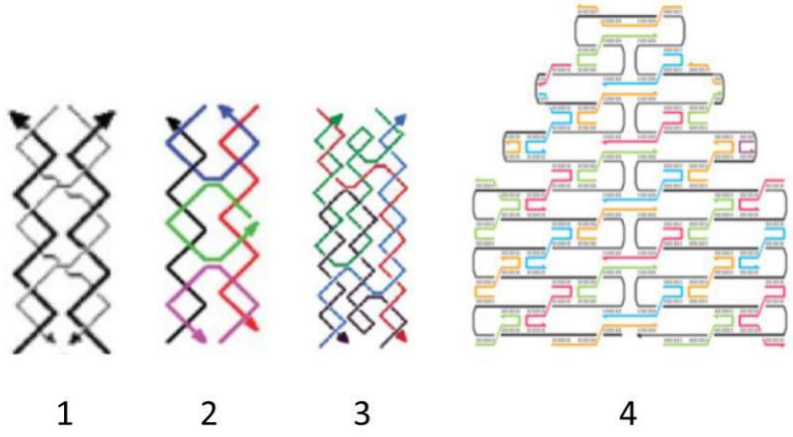

Figure 3. Models of some representative DNA tiles: DNA double-crossover (DX) tile, formed through strand exchange between two DNA duplexes (9);[29] more rigid DX tile, constructed using five strands (10);[18f] more rigid DNA triple-crossover (TX) prepared using three helices (11);[30] DNA origami motif consisting of a viral DNA strand, folded into desired bi- or tri-dimensional nanostructures (12).[28] The oligonucleotides are shown as simplified backbone traces. Adapted from ref [29] by permission of the publisher Taylor & Francis Ltd, http://www.tandfonline.com, Copyright 2000; from ref [18f] with permission from The Royal Society of Chemistry, Copyright 2005; from ref [30] with permission from American Chemical Society, Copyright 2003; from ref [28] by permission from Springer Nature, Copyright 2006.

The folding takes place through the use of judiciously chosen short complementary nucleic acid sequences, which appropriately "staple" the viral DNA, forming the desired nanostructure. The design of the so-called staple units is thus solely responsible for the precise geometries of the nanostructures. DNA origami tiles are basically large versions of DX motifs, as they essentially contain many parallel double helices, rather than two.Based on the DX strategy, *Liu et al.* have described DNA arrays of finite, defined and controlled size.[31] One of the networks that they have reported made use of a total of twenty-five DNA tiles, of which only thirteen were different, as several tiles could be used in multiple positions in the array (Figure 4). Each tile consisted of eight DNA double helices joined together in a plane with two crossovers to connect to adjacent helices (Figure 4a). The same core strand sequences were used in all the thirteen different tiles; the only differences were the sequences of the sticky ends emerging from the helical axis of the tiles and used to lead the self-assembly of the system. The arrays (Figure 4b) were constructed in a stepwise manner: the individual tiles were first formed by annealing a stoichiometric mixture of the component DNA strands to 90 °C, and slowly cooling to 40 °C. The resulting thirteen DNA tiles were then mixed in the correct proportions at 40 °C and, upon cooling the solution to 10 °C, the arrays were formed. A sample of the solution was deposited onto a mica surface and imaged by AFM (Figures 4c,d), revealing a total size of array of 110 110 nm^2.

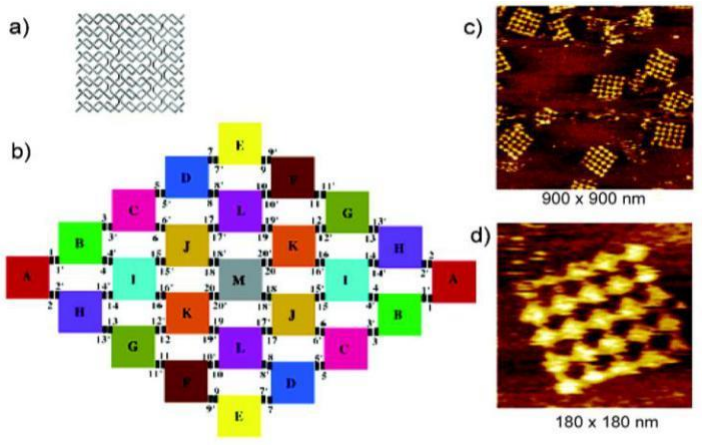

Figure 4. a) The 8-helix tile showing the crossover points. b) The array design using thirteen different tiles (each bearing different sticky ends) to form the 5 5 array in a predictable and controllable manner; c-d) AFM images of the twenty-five tile array on mica.[31] Adapted from ref [31] with permission from American Chemical Society, Copyright 2005.

While *Liu et al.* described the formation of finite-size arrays, the groups of *Yan* and *LaBean* reported the use of four interconnected four-arm DNA junctions to form two-dimensional nanogrids, which extended up to several hundred nanometres on each edge (Figure 5).[32] The individual units used to form the networks resembled a four-point star and were made up of nine DNA single strands, with one of the strands participating in all four junctions (Figure 5a). The design of the sticky ends at the apices of the four-point star was based on a "corrugated" strategy. Through this approach, adjacent tiles associate with one another in a way that the same face of each tile is alternately oriented up and down in neighbouring tiles (Figure 5b). This was done to ensure that the curvature inherent in each tile is cancelled out within the assembly, leading to flat arrays. The complexes were formed

by mixing a stoichiometric quantity of each strand, after which the mixtures were slowly cooled from 90 to 20 °C over 16 h. Following the deposition of the solution onto a mica surface, the formation of extended square two-dimensional arrays with 19 19 nm^2 pores were observed by AFM (Figure 5c).

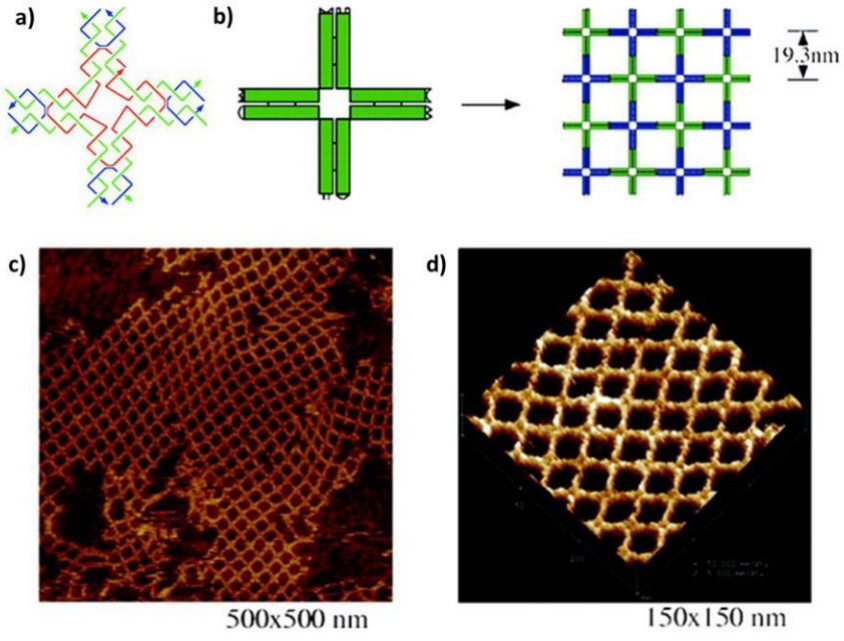

Figure 5. Self-assembly of four interconnected four-arm DNA junctions. a) The four-point star motif (which can also be mentioned as a 4 4 tile strand structure). It contains nine oligonucleotides, shown as simplified backbone traces. The four-arm junctions are oriented perpendicular to each other; the red strand participates in all four junctions. b) Self-assembly of two-dimensional networks with the corrugated design. The tiles have two surfaces; one faces out of the plane (in green), the other faces into the plane (in blue, when visible). c-d) AFM images of the resulting two-dimensional arrays formed on mica; d) surface plot of a magnified region from c).[32] Adapted from ref [32] with permission from The American Association for the Advancement of Science, Copyright 2003

Upon obtaining the desired two-dimensional network (Figure 5c-d), *Yan et al.* used the nanogrid to template the protein streptavidin into periodic arrays,[32-33] by incorporating a biotin group[34] into the four-

point star design, at the tile centre (Figure 6a). When streptavidin was then added to the solution of the resulting self-assembled network, its interaction with biotin led to a protein array (Figure 6b).[32] Streptavidin has a diameter of ~5 nm, therefore its binding to the DNA nanogrids generates bumps at the centre of the 4 4 tiles, which can be compared with regions where there is no protein-ligand binding, as it can be seen on the AFM images in Figure 6b. Afterwards, the same DNA network has been used to organize 5-nm gold nanoparticles (Au NPs) into periodic square lattices.[35]

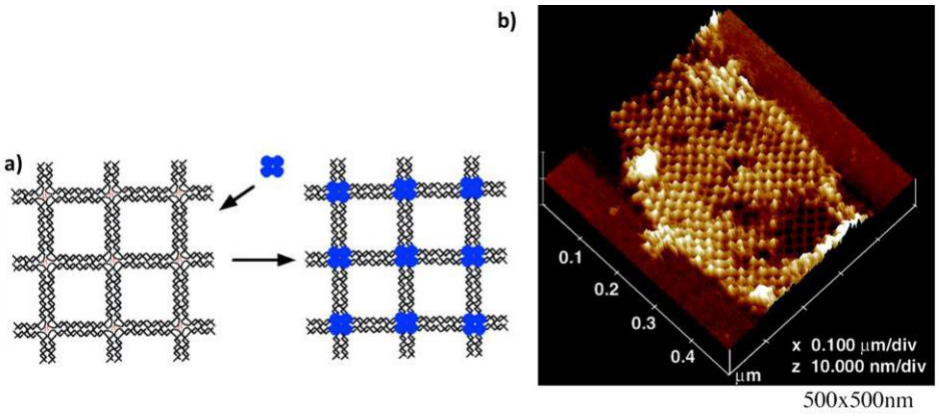

Figure 6. Self-assembly of protein arrays, templated by the two-dimensional network previously obtained using four interconnected four-arm DNA junctions with the corrugated design (*Figure 10*). a) Schematic drawing of the DNA nanogrids scaffolded assembly of streptavidin. (Left) DNA arrays, in which biotins (yellow dot) were incorporated into the four-point star design, at the tile centre. (Right) Binding of streptavidin (blue tetramer) to biotin, resulting in protein nanoarrays on DNA lattices. b) AFM image of the self-assembled protein arrays.[32] Adapted from ref [32] with permission from The American Association for the Advancement of Science, Copyright 2003

Similar to the results by *Yan* and co-workers, extended porous networks on surfaces have also been observed by varying the DNA tile to a three-point star,[36] a five-point star[37] and a six-point star.[38] In their report, the group of *Mao* used a three-point star motif to engineer

extended, highly ordered, two-dimensional crystalline arrays with domains as large as 1 mm in length, and pores of 30 nm (edge-to-edge) (Figure 7a-d).[36] They used the resulting DNA networks as masks to fabricate metallic nanostructures by vapour-depositing a thin film of Au (20 nm thick) against the DNA lattices supported by mica and then mechanically lifted them off. AFM analysis of the gold replicas showed that the hexagonal DNA patterns were accurately replicated into Au (Figure 7e-g).[36]

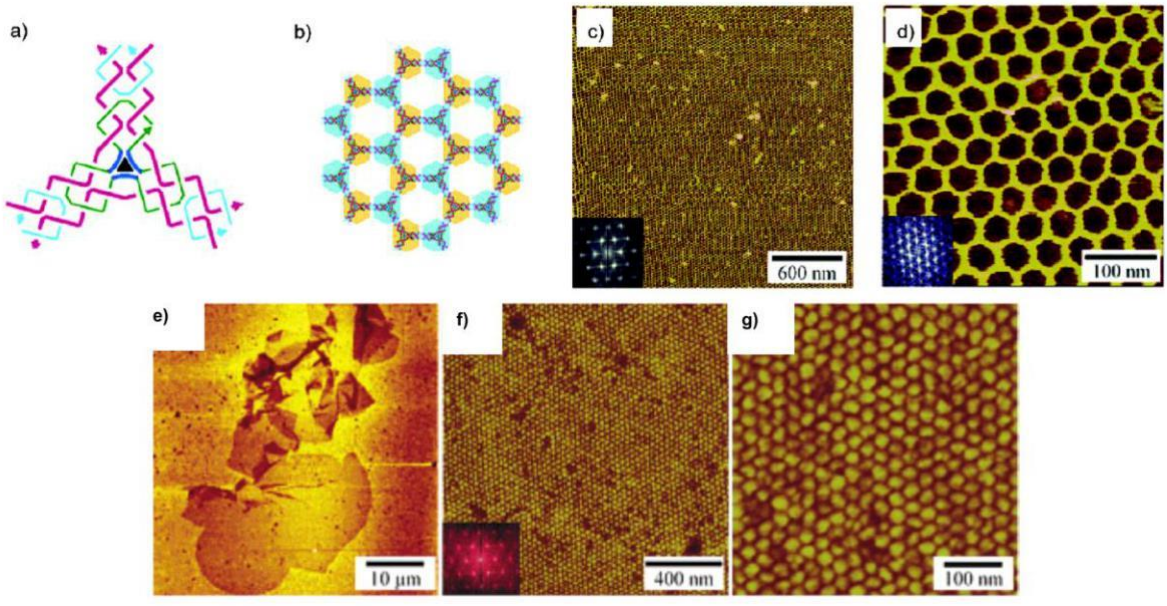

Figure 7. a) The three-point star motif made up of seven DNA single strands. **b)** Model of the two-dimensional array which would be expected by the assembly of the individual tiles. **c-d)** AFM images of the self-assembly on mica, showing the resulting extended and highly ordered hexagonal porous network. **e-g)** AFM analysis of gold replicas, constructed with the DNA two-dimensional arrays as templates.[36] Adapted from ref [36] with permission from American Chemical Society, Copyright 2005.

By exploiting the same strategy, *Majumder et al.* designed and built "double-decker" tiles which afforded the self-assembly of two-

dimensional networks, extending over tens of micrometres in size (Figure 8).[39] The double-decker tiles consist of two four-point stars lying one on top of the other, and linked by two crossovers in each arm, arranged perpendicular to the plane of the tile (Figure 8a). The sequence composition of each arm was the same, making the four arms of the double-decker symmetric. This afforded a simpler sequence design and the reduction of the required number of DNA strands. Furthermore, it has been demonstrated that sequence symmetry lead to the formation of large lattices.[40] As in previous examples, the sticky ends were programmed to create corrugated associations between neighbouring tiles (Figure 8b). The self-assembly of the network was formed by annealing a stoichiometric mixture of the strands to 90 °C, and slowly cooling to 20 °C over 16 h, followed by overnight incubation at 4 °C. Following deposition on a mica surface, AFM analyses of the resulting assembly showed the formation of large arrays, extending over tens of micrometres and displaying porous cavities (edge-to-edge) 30 nm long (Figures 8c,d). The main advantage of these double-decker tiles is that the sticky ends can be designed in such a way that a three-dimensional periodic lattice can be formed. Such a lattice would present cavities of substantial size, with a periodicity of ~60 nm. The latter could be used for precise hosting of guest macromolecules and nanostructures, such as proteins or nanoparticles. Since DNA assemblies are delicate and fragile, they tend to deform or break into small pieces due to the shear forces occurring during the solution-to-surface transfer.

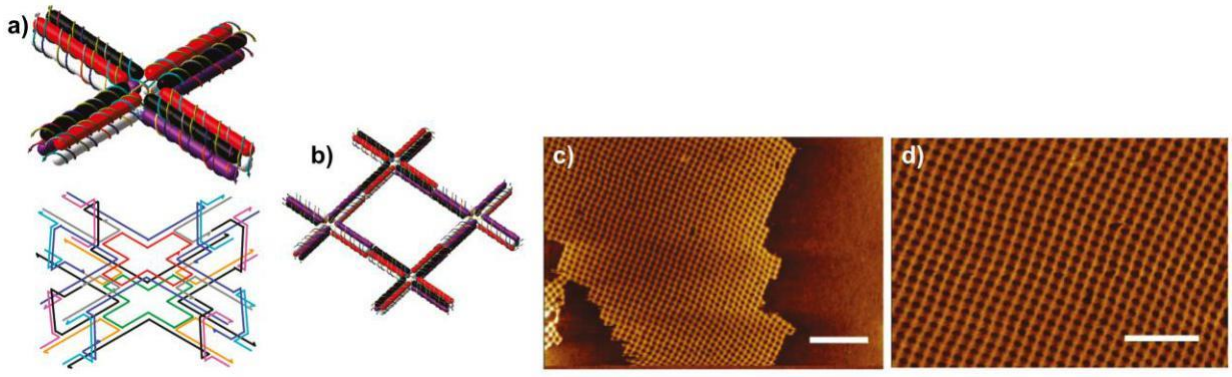

Figure 8. a) Top: schematic representation of the double-decker tile; bottom: schematic drawing of the strand trace through the tile. b) Expected self-assembly of the double-decker tile into two-dimensional networks, using the corrugated design. c-d) AFM images of the resulting double-decker two-dimensional array, with corrugation; c) scale bar, 300 nm; d) scale bar, 200 nm.[39] Adapted from ref [39] with permission from American Chemical Society, Copyright 20011.

To overcome this issue, *Mao* and co-workers[41] developed an *in-situ* strategy for self-assembly DNA directly on solid surfaces, using the same three-point star motif as that previously described (Figure 7). The protocol involved the assembly of the individual tiles by first annealing in solution the single stranded DNA strands to 95 °C, and slowly cooling to 60 °C, and then assembling the tiles into two-dimensional network on the mica surface by incubation at 50 °C for 16 h (Figure 9a). The critical temperatures in this two-step assembly were 60 and 50 °C. Indeed, cooling to 60 °C in solution was low enough to allow the formation of the individual tiles but not their further assembling into large two-dimensional arrays. On the other hand, at 50 °C and on the solid mica surface, the surface stabilisation of DNA tiles resulted in nuclei, which initiated the further assembly of DNA

tiles into large two-dimensional nanogrids, covering the entire surface (Figure 9b). As it can be seen comparing the AFM images in Figures 7d and 9b, the resulting assembly was similar to that previously obtained in solution. By using the same strategy, they also showed that, more flexible tiles were flattened due to their interactions with the surface, and therefore formed micrometre extended periodic networks. These structures could not be obtained in solution.

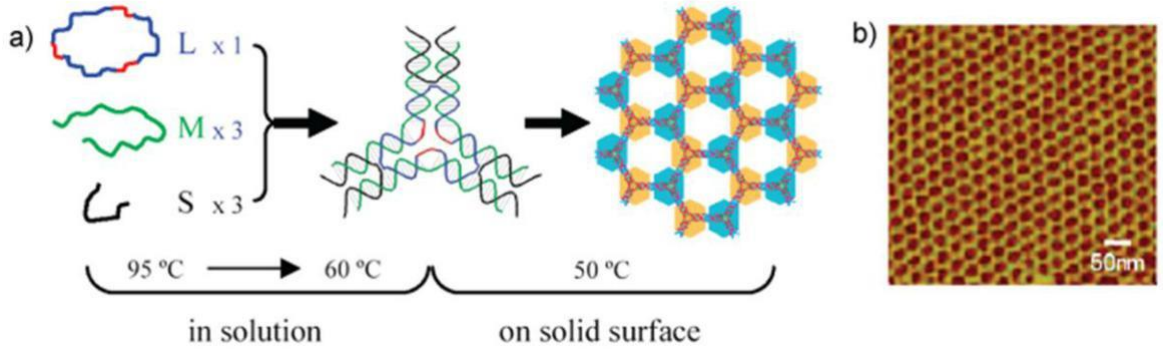

Figure 9. a) Schematic representation of the assembly of the two-dimensional array in two steps. First, the individual tiles were formed in bulk solution from 95 to 60 °C, next the large two-dimensional crystals were assembled on solid surfaces. The three-point star tile contains seven strands. b) AFM image of the self-assembly of DNA, showing the porous network on a mica surface.[41] Adapted from ref [41] with permission from American Chemical Society, Copyright 2009.

More recently, *Yan* and co-workers[42] have demonstrated that complex 2D Archimedean tile-type lattices, with micrometre scale dimensions, could be obtained by using a combination of programmed three- and four-arm DNA junction tiles (Figures 10a-b). Since Archimedean tiles, which are periodic "mosaics" obtained by placing regular polygons edge to edge around a vertex, are composed of more than one type of regular polygon,[43] at least two different building blocks are required for

their formation. Hence, both the geometry and dimensions of the final desired tiling and the properties of the 3D ds-DNA structure must be taken into consideration for the design of spatially compatible components. By using three-arm and four-arm tiles of the same length but with different sticky ends, they were able to obtain two different patterns, the "Cairo" and the "Prismatic" pentagonal tiles (Figures 10a and 10b respectively). The nanostructures were formed in solution by a one pot-annealing of the single strands mixed in the designed ratio, cooling from 95°C to 4°C over 12 hours. They were then transferred into mica and visualized by AFM (Figures 10c-f), which showed that both had often curved edges, with the second forming large 2D sheets that curled up into tube with 80 to 250 nm diameters (Figure 10f). This was attributed to the tiles facing all the same direction and therefore the curvature of every single tile was propagated to the whole array.

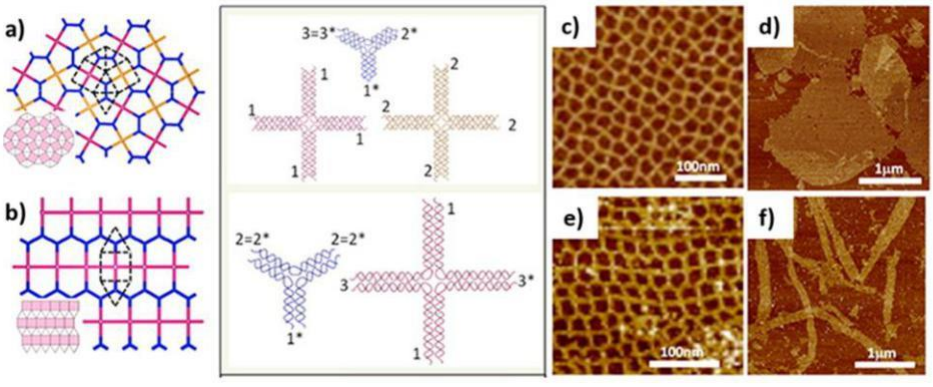

Figure 10. Sticky-end matching rules for two Archimedean tiling designs and for the complex DNA network. a) Cairo pentagonal tiling. d) Prismatic pentagonal tiling and relative AFM images at two different resolution b-c) and e-f).[42] Adapted from ref [42] with permission from American Chemical Society, Copyright 2013.

Later,[44] they showed that, by using multi-arm DNA junctions with reduced geometric symmetry and appropriate matching sticky ends, even more complex ordered 2D patterns could be obtained (Figures 11a). Hierarchical annealing and surface mediated growth were used to facilitate the formation of larger networks and a corrugated design was employed for the more complex structure. Ordered 2D arrays of hundreds of nanometers size could be formed (Figure 11b). The use of a hierarchical stepwise folding, where the two units were annealed separately and then mixed together at 25 °C, reduced the possibility of mismatches between the building units leading to the formation of large (up to several microns) 2D lattices (Figure 11c).

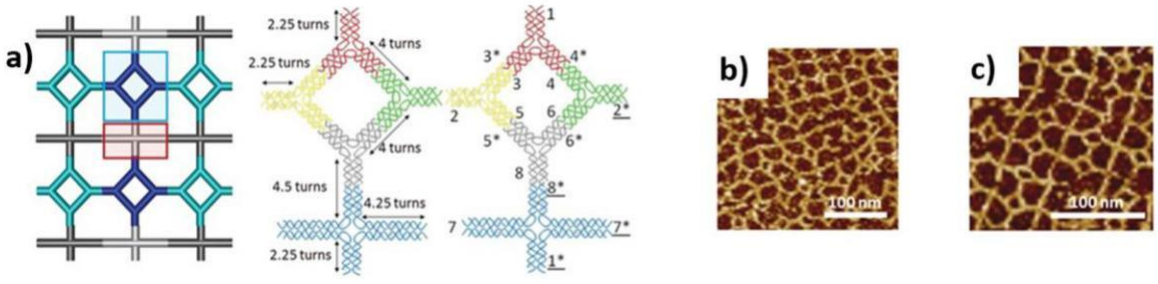

Figure 11. a) Schematic of the pattern for the complex DNA network and its two units (in blue and red boxes) with optimized arm length (left) and matching rules (right) for the specific motifs. b-c) AFM images for the one pot annealing product and after the second step of the hierarchical folding strategy.[44] Adapted from ref [44] with permission from WILEY‐VCH Verlag GmbH & Co. KGaA, Weinheim, Copyright 2016

Seeman and co-workers[45] described the formation of well-ordered two-dimensional DNA arrays (whose dimensions reached 10 m), obtained by the self-assembly of two double-layer DNA-origami tiles, displaying two orthogonal domains (Figure 12). In that work, two complementary tiles

A and **B** were prepared (Figure 12a). Each one consisted of two helix axes, which propagated in two independent directions perpendicular to each other, one in a plane above the other (Figure 12b). Bringing complementary **A** and **B** together, as the two layers of each DNA-origami have opposite orientations relative to the plane, each tile interacted with the adjacent one oriented at 90° with respect to each other. In this way, the top layer of one tile was linked to the bottom layer of the next.

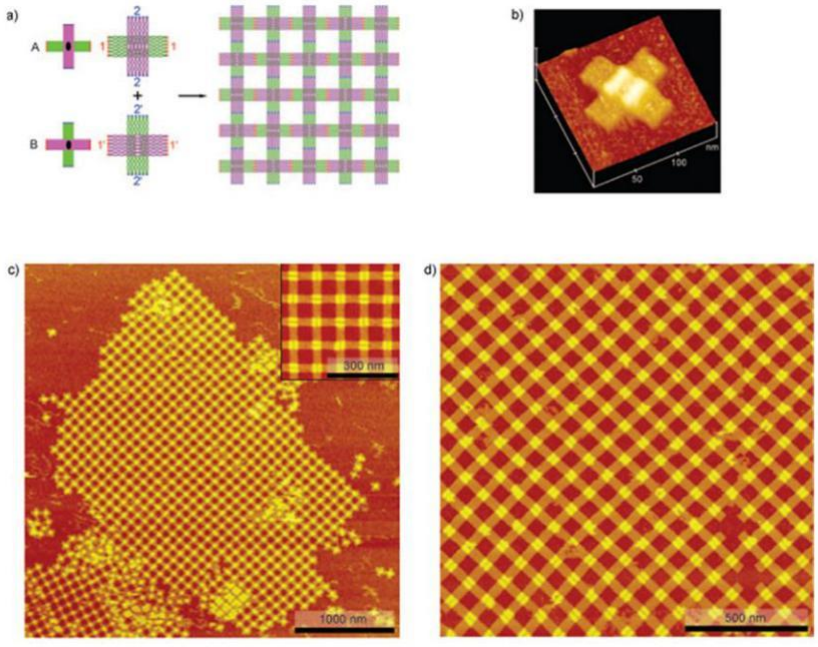

Figure 12. a) Schematic structure of the tiles A and B. The purple pink rectangular domain lies above the green rectangular domain in both tiles. Apart from the sticky ends, both tiles were identical. b) AFM image of a woven pattern individual tile. c-d) AFM images of the self-assembled porous network on a mica surface, formed by the two tiles upon annealing at 53 °C.[45] Adapted form ref [45] with permission from WILEY‐VCH Verlag GmbH & Co. KGaA, Weinheim, Copyright 2010

The resultant alternating self-assembly had the appearance of a braided

pattern, as it can be observed on the AFM images displayed on Figures 12c and 12d. The annealing temperature required for the formation of the desired self-assembly was 53 °C. Lower temperatures resulted in aggregates of the tiles and higher temperatures damaged the tiles preventing the self-assembly from forming.

Subsequently, cross shaped DNA origami tiles have been used to build 2D ordered porous frameworks by "lipid-bilayer-assisted self-assembly". DNA origami were electrostatically adsorbed on a mica-supported zwitterionic lipid bilayer in the presence of divalent cations, such as Mg^{2+},[46] and the 2D networks (Figure 13a-b) assembled either via sticky ends or blunt ends stacking interactions (i.e. binding of DNA duplex termini due to base stacking).[47] Origami tiles can be designed to have multiple helices geometrically arranged so that multiple blunt ends can give rise to cooperative binding and direct self-assembly. The cavities in the network were used to dock square origami tiles (SQ-Origamis) of fitting dimensions.[48] This process was studied by high speed AFM and a dynamic adsorption/desorption behavior of the SQ-origamis was observed. The SQ-origami tiles could be more strongly held into the cavities by increasing the Mg^{2+} concentration or by introducing sticky-ended connectors both in the SQ-origamis and the frameworks tiles. By using a sequential approach, the authors were able to obtain a checkerboard-like pattern, where the SQ-origami were trapped only at every other cavity (Figure 13c).

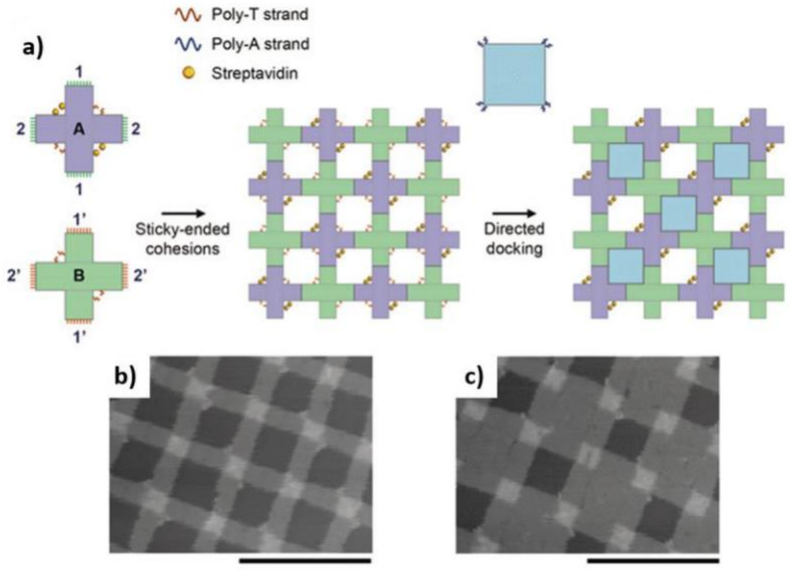

Figure 13. a) Schematic of the sequential self-assembly of the framework from two components and directed docking of SQ origamis. b-c) AFM images of the 2D DNA origami frameworks and of the checkerboard-like pattern. Scale bars, 200 nm.[48] Adapted from ref [48] with permission from WILEY‐VCH Verlag GmbH & Co. KGaA, Weinheim, Copyright 2018

In a first step, they assembled the network using two different types of tiles, which were designed to alternate in the arrangement, and which contained protruding sticking ends connections for the docking of the SQ-origami only in determined positions. Then, in a second step, they added the SQ-tiles which were docked into positions by sticky end interactions (Figure 13a).

Recently, *Ke* and co-workers[49] described honeycomb 2D flat lattices up to 6x9 μm^2 dimensions, obtained from hexagonal DNA-origami tiles (HT, Figure 14). They designed a series of hexagonal tiles (Figure 14a) that assemble into honeycomb lattices, which could form either flat 2D lattices or tubes. To form the flat porous networks, they have

In particular, they engineer eight helix hexagonal tile (2 × 4 HT) using connector strands that contained 1-bp sticky-ends and one unpaired scaffold bases between each pair of connected DNA duplexes (Figure 14b). Exploiting the 2×4 HT based DNA-origami tubes and lattices as platform for plasmonic materials, they formed ordered and organised arrays of Au NPs, which were anchored through single protruding strands within the tiles plane (Figure 14d).

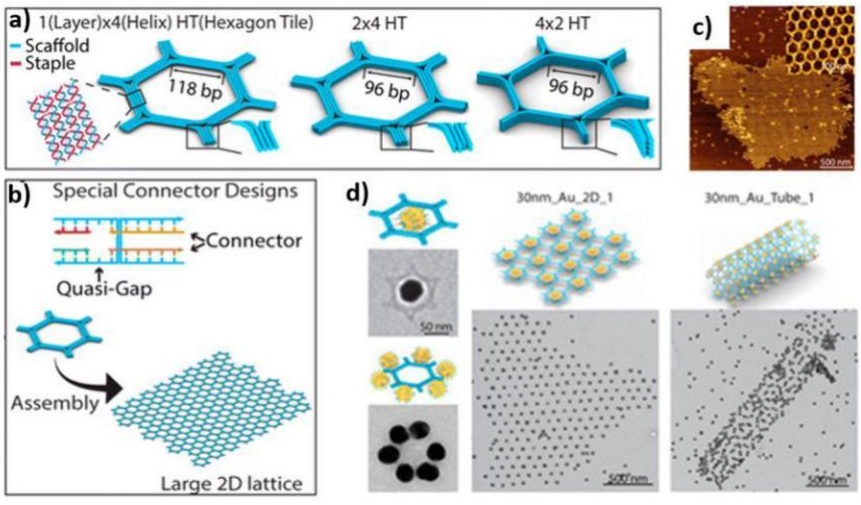

Figure 14. a) Schematics of DNA-origami hexagon tiles of the 1 × 4 HT, 2 × 4 HT, and 4 × 2 HT. Insets show that each cylinder represents a DNA duplex and connectors more in details. b) Connector modification to facilitate the formation of 2D lattices. c) AFM image of large 2D lattices assembled from the 2 ×4 HT using 1-bp-quasi-gap connectors. d) 30 nm AuNP monomer (top) and hexamer (bottom) assembled on a hexagon tile; 30 nm AuNP superlattices assembled on hexagonal 2D lattices and tubes occupying type-1 cavity.[49] Adapted from ref [49] with permission from American Chemical Society, Copyright 2016

In a parallel approach, *Gopinath* and *Rothemund* reported the electrostatic self-assembly of triangular DNA origami onto lithographically defined binding sites on Si/SiO_2 substrates (Figure 15a-b).[50] The electrostatic DNA-surface bonds were then successfully

converted to covalent bonds through the use of cross-linking reagents. Binding sites of the same shape and size as triangular origami were first patterned on SiO_2 substrates in a way that silanol groups, which were further ionised at an appropriate pH to become negatively charged, were created at each site. A solution of origami was then deposited onto the substrate, and the Mg^{2+} present in the buffer provided the electrostatic bridges between the ionised silanols and the negatively charged origami (Figure 15a). Studying various global (origami and Mg^{2+} concentrations, pH, incubation time) and spatial (binding site size and spacing) parameters, *Gopinath* and *Rothemund* could optimise the self-assembly of the DNA origami on the substrate, affording single-origami binding at 94 4% of sites (Figure 15b).

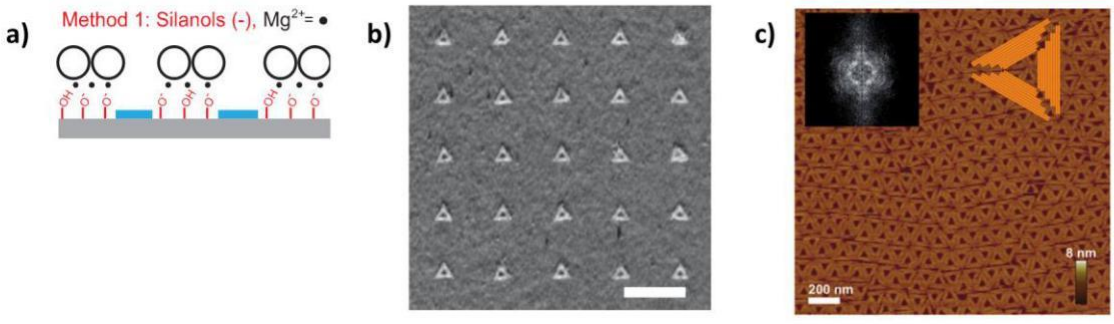

Figure 15. a) One of the reported method placement, described herein as example: at an appropriate pH, surface silanols become negatively charged and divalent Mg_{2+} cations, contained in the DNA origami buffer, act as a bridge to immobilise the negatively charged DNA origami (represented by black circles). b) AFM image after placement of 110 pM of triangular DNA origami at pH 8.3 in a 35 mM concentration of Mg_{2+}, during 60 min of incubation. The AFM image shows mostly well-oriented single origami. Scale bar, 400 nm;[50] c) AFM image of the mica surface-assisted assembly of triangular origami tiles, deposited from a buffer solution containing both Mg_{2+} and Na_{+} cations. The resulting self-assembly shows extended ordered arrays, with a trigonal symmetry. The measured dimensions of the tiles are 126 nm per side, and the wavy structure is due to dislocations.[52] Adapted from ref [50] (https://pubs.acs.org/doi/10.1021/nn506014s) with permission from American Chemical Society, Copyright 2014 (further permissions related to the material excerpted should

They also observed that surface diffusion played an important role in the binding mechanism. Their strategy allowed a lower working Mg^{2+} concentration than previous studies,[51] which is important for the application to nanodevices as most devices aggregate at high Mg^{2+} concentration. Mg^{2+}-free conditions were also achieved upon covalent stabilisation of the origami nanoarrays on the surface (*via* isourea or amido bond formation).

Similarly, the group of *Simmel* reported the assembly of DNA origami into extended highly ordered close-packed arrays (Figure 15c).[52] Their strategy was based on an electrostatic control of the adhesion and mobility of the DNA structures onto mica surfaces, by simple addition of monovalent cations. Indeed, as previously mentioned, adsorption of DNA origami onto mica is mediated by Mg^{2+} ions, contained in the origami folding buffer, which act as salt bridges between mica and DNA. The addition of monovalent ions such as Na^{+} to the buffer can weaken this interaction by partially replacing the Mg^{2+} ions, affording a more diffuse charge layer between the surface and the polyelectrolyte solution of DNA. As a result, DNA origami structures become mobile on the surface and associate with each other into close-packed structures dominated by steric repulsion. Among the reported examples, the authors described the mica surface-assisted assembly of triangular origami tiles, deposited from a buffer solution containing both Mg^{2+} and Na^{+}

cations, into extended ordered arrays with a trigonal symmetry (Figure 15c). Subsequently, these arrays were used by *Keller* and co-workers[53] as molecular lithography masks to form regular proteins patterns over large surface areas (Figure 16). Negatively charged proteins in Mg^{2+}-containing buffer were directly adsorbed into the voids of the origami tiles. The surface coverage could be tuned from single proteins to densely packed protein monolayers by adjusting the protein and Mg^{2+} concentrations.

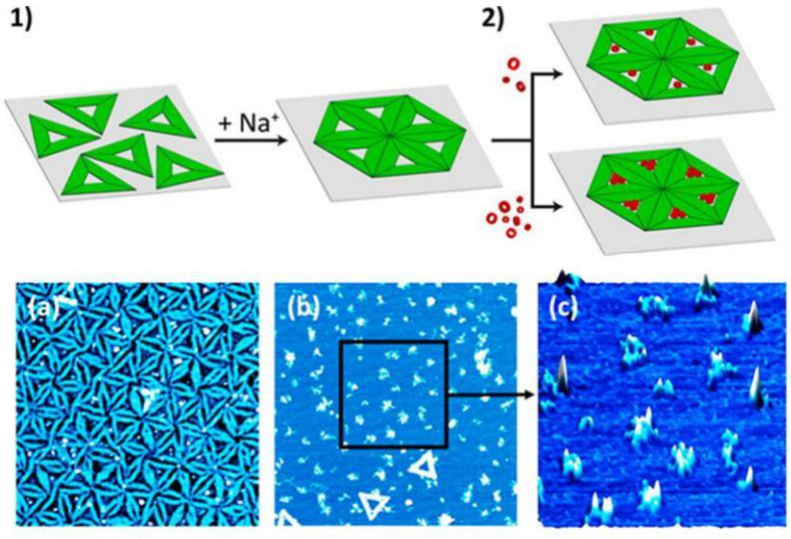

Figure 16. Procedure for the formation of regular protein patterns on surfaces and AFM images. 1) Assembly of a densely packed monolayer of triangular DNA origami tiles, 2) adsorption of proteins on mica within the holes of the DNA mask. The number of proteins within the holes increases with increased protein concentration and depending on buffer conditions. a) AFM image of BSA adsorbed on the exposed mica surface masked by the triangular DNA origami tiles b) BSA pattern on mica after desorption of the DNA origami mask. Images sizes are 1.1 × 1.1 µm2 c) 3D zoom of the square region indicated in b). Image size is 0.5 × 0.5 µm2 and height scales are 2nm.[53] Adapted from ref [53] with permission from American Chemical Society, Copyright 2016

This approach was quite versatile, and they were able to form regular patterns using four different shape and molecular weights proteins. Two single strand annealing proteins Red*β* and Sak (SSAPs), ferritin and

bovine serum albumin (BSA) were successful patterned on mica surfaces. An example is the resulting pattern obtained with BSA (Figure 16c), which was formed by 15 minutes incubation of the mica supported origami array in B1 buffer with 30 mM Mg^{2+} and 5 µM BSA, followed by 30 minutes incubation in TAE buffer with 200 mM NaCl (Figure 16).

When Simmel and co-workers used the same assembly approach with the cross-shaped origami tiles described by *Seeman* and co-workers (Figure 12a),[45] a lower degree of order and disintegration of the close packing were observed at Na^{+} concentrations above 200 mM. Thus, to form extended ordered porous domains, they used modified blunt-ended[47] tiles, which interactions would allow self-repairing and reorganization of the forming lattice through reversible bonds formation. In this way crystalline arrays with the micrometre-range size were obtained.[52]

Finally, moving away from the crossover junctions used in the above examples, *Hamada et al.*[54] demonstrated that the assembly of a variety of structures on surfaces (1D ladders, 2D porous networks and polar coordinated wheels) was possible using single-duplex-based T-shaped junction tiles. This was the first report to introduce T-junctions (Figure 17a) into the field of DNA nanotechnology. Unlike the more commonly used crossover junction, the T-junction is right-angled. This provided the possibility of preparing a larger variety of DNA nanostructures. Also, the resulting more rigid junction leads to more stable assemblies.

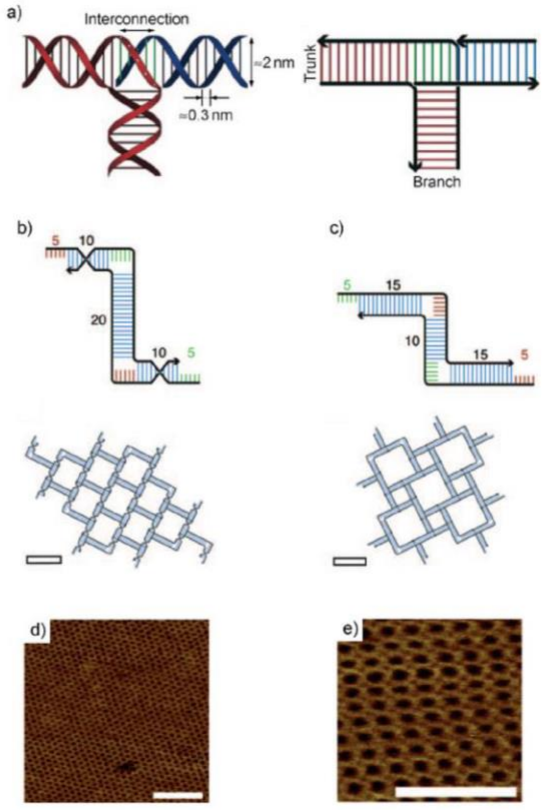

Figure 17. a) Helical and schematic representations of the single-duplex-based T-shaped junction. b) Schematic representation of the T-shaped junction tile used to form the two-dimensional brick-wall lattice and the model of the expected self-assembled structure, following annealing and cooling. c) schematic representation of the T-shaped junction tile used to form the two-dimensional windmill lattice and the model of the expected self-assembled structure, following annealing and cooling. d-e) AFM images of the resulting self-assembled structures on mica surfaces. Scale bar, 100 nm.[54] Adapted from ref [54] with permission from WILEY‐VCH Verlag GmbH & Co. KGaA, Weinheim, Copyright 2009

Last but not least, the individual tiles can be of a smaller size, therefore, the resultant assemblies can have a higher resolution *i.e.* smaller unit cell and thus greater nanoscopic detail. Figures 17b-e show two types of two-dimensional self-assembled DNA networks that were observed upon the mica-assisted self-assembly of two types of tiles with T-junctions. Recently, the group of *Mao* demonstrated the self-assembly of DNA arrays through the use of a unified T-Junction, built

from one short DNA strand only (Figure 18).[55]

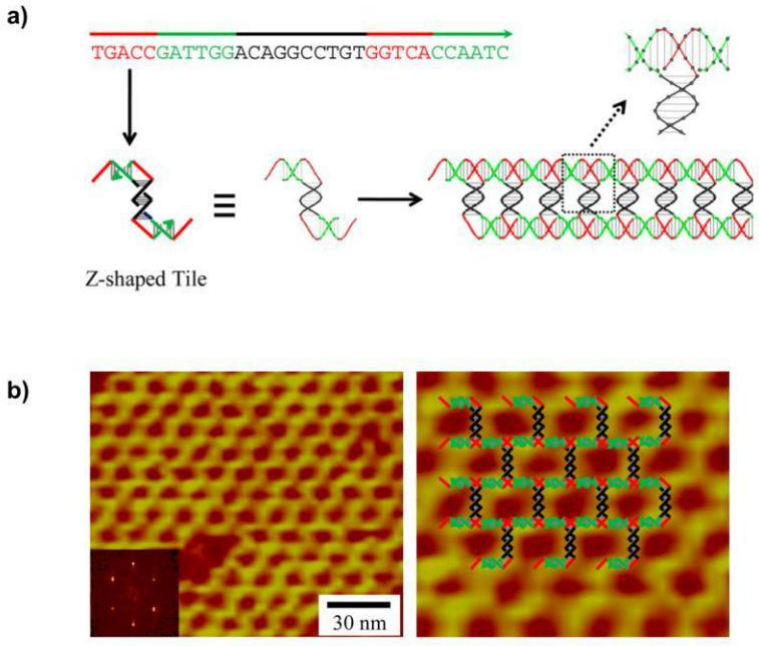

Figure 18. Self-assembly of two-dimensional networks from symmetric bulged DNA duplex motifs. **a)** The motif consists of the association of two unique identical DNA strands, and each strand contains five segments. Upon dimerisation of the system, remaining single-stranded DNA (in red) behave as sticky ends and lead to the assembly of the motifs into periodic arrays. **b)** AFM image of the DNA two-dimensional networks obtained by mica surface-mediated self-assembly. Left: the inset is the corresponding Fourier transformation pattern of the image. Right: close-up view of the left image, superimposed with a schematic drawing of the DNA two-dimensional network.[55] Adapted from ref [55] with permission from American Chemical Society, Copyright 2014

This derives from what has been defined a "minimalist's approach of DNA tiles self-assembly",[20g] which being based on the self-assembly of highly symmetric DNA sequences and structures, allows the use of the minimum numbers of different DNA strands and tiles to build nanostructures. The motif consists of the association of two unique identical DNA strands, and each strand contains five segments (Figure 18a): a central palindromic sequence (black) whose homo-dimerisation forms the central helical domain, two green complementary sequences

whose hetero-dimerisation forms two flanking helical domains, and two red complementary sequences that remain single-stranded in symmetric motifs and consist of sticky ends. The sticky ends thus form the T-junctions upon hybridisation, and lead to the assembly of the motifs into periodic arrays. Large two-dimensional arrays were successfully formed by mica-surface-mediated assembly, as it can be observed by AFM (Figure 18b). This strategy uses DNA palindromic sequences, which could form either the programmed intermolecular homo-dimer or an intramolecular hairpin. When long sequences are employed, this could be a problem, as the intramolecular hairpin formation would be favored. To overcome this issue, the group of *Mao*[56] developed a DNA self-assembly strategy that exploit the intramolecular hairpin formation by using the bubble cohesion interaction[57] between interior loops of two DNA duplexes through complementary Watson-Crick base pairing. They designed single-stranded DNAs, which could quickly fold to form three-valent hairpins associating with three other hairpin motifs via two different mechanism (bubble cohesion and T-junction) to form 1D ladders or 2D arrays (Figure 19). The DNA homodimers contain six-base-long interior loops with self-complementary sequences for the bubble cohesion, but also an overhang and a bulge with complementary sequences which allow the T-Junction formation and the polymerization into nanostructures.

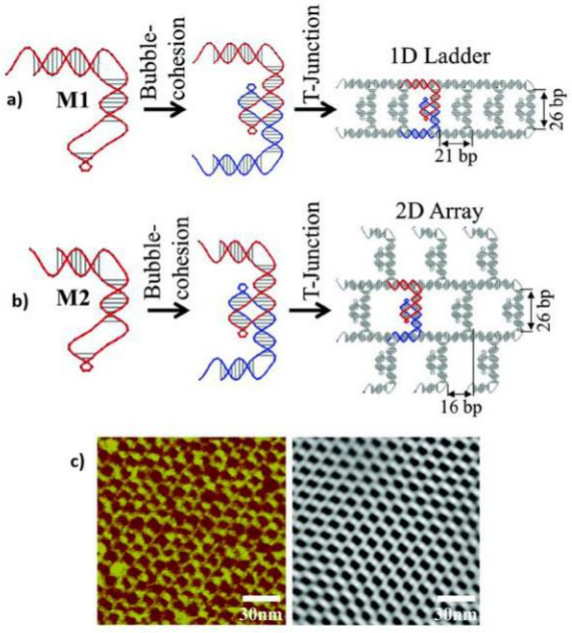

Figure 19. Self-assembly of one-stranded DNA hairpin motif **M**. The motifs contain self-complementary, interior loops that hybridize with each other *via* bubble-cohesion forming C-shaped homodimers, which further associate with each other *via* T-junction cohesion into large nanostructures. **a)** 1D ladders (from motif **M1**) and **b)** 2D arrays (from motif **M2**). For each homodimer, the two component motifs are coloured differently for clarity. The determining factor for the final structure (1D ladder or 2D array) is the length of the horizontal helix domain. **c)** AFM analysis and a FFT-reconstructed image (gray scale picture) of the zoom-in AFM image of self-assembled DNA 2D arrays.[56] Adapted from ref [56] with permission from The Royal Society of Chemistry, Copyright 2017

The length of the horizontal helical domain dictates the association into 1D ladders (even number of helical half-turns, Figure 19a, e.g. 21 bps long) or 2D arrays (odd number of helical half-turns, Figure 19b, e.g. 16 bps long). The DNA nanostructure were assembled by mica-surface-mediated assembly and imaged by AFM (*Figure 19c*).

Yin and co-workers[58] described a different approach to build porous micrometer size 2D DNA crystals with defined depth (Figure 20). They employed previously reported[59] DNA structures built using single-stranded DNA bricks. Each brick is composed of a different 32-nt strand

with four 8-nt binding domains, so that, when included in the final intended structure, they adopt the shape of two 16-nt antiparallel helices connected by a single phosphate linkage. The two pairs of domains within the brick are named head and tail (Figure 20a).

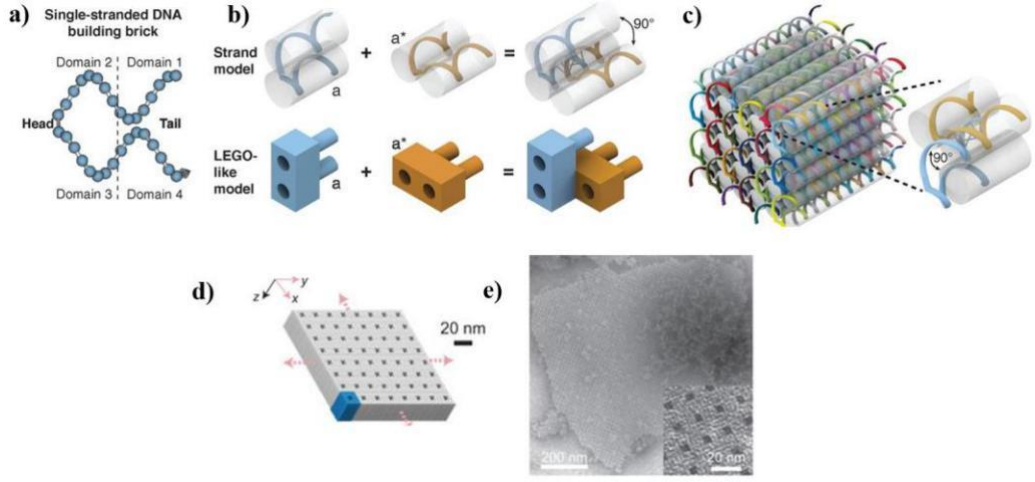

Figure 20. Design of DNA brick structures and self-assembly into 2D crystals. a) A 32-nt four-domain single-stranded DNA brick. Each domain is 8 nt in length. The connected domains 2 and 3 are indicated as "head"; domains 1 and 4 are the "tail". b) Two-brick assembly showing the 90° dihedral angle formed via hybridization of two complementary head domains "a" and "a*" and analogous LEGO® models. c) A molecular model showing the helical structure of a 6H by 6H by 48B cuboid 3D DNA structure. Each strand has a particular sequence, as indicated by a distinct colour. The inset shows a pair of bricks.[59] d) Infinite-size DNA crystals built with DNA bricks cylinder model and e) TEM image.[58] Adapted from ref [59] with permission from The American Association for the Advancement of Science, Copyright 2012 and ref [58] by permission from Springer Nature, Copyright 2014

When a head domain interacts with complementary tail domain on a neighbouring brick, they associate forming three parallel helices with a resulting 90° dihedral angle (Figure 20b). As an example, the 6H (helix) × 6H (helix) × 24B (base pair) cuboid structure that can be designed to grow along three orthogonal axes is illustrated in Figure 20c. By opportunely designing the component bricks, crystals with

complex 3-dimensional features, such as cavities and channels, could be formed. Each crystal was assembled via non-hierarchical growth, by one-pot annealing, for 72 h or 168 h, of a roughly equimolar ratio mixture of unpurified DNA brick strands in the presence of 40 mM $MgCl_2$. The assembled crystals were imaged using transmission electron microscopy (TEM), cryo-electron microscopy (cryo-EM) or AFM.

Porous networks through self-assembly of peptide structures.

Amino acids sequence in peptides and proteins contain the information that determines their structure, properties and function and directs their self-assembly by specific interactions, mainly by H-bonding motifs. Therefore, by programming amino acids sequences, it is possible to rationally design peptides that can act as multifunctional building blocks for engineering bio-inspired nanostructures on surfaces. The possibility of sequence variation by combining the 20 standard amino acids is vast and makes self-assembly prediction and rational design difficult.

Peptide-based networks. Most STM studies of peptides have been devoted to small oligopeptides and to the investigation of the underlying molecular mechanism of the association into fibrils of amyloid oligopeptides involved in neurodegenerative processes, such as Alzheimer's and Parkinson's diseases. These oligopeptides tend to assemble in close packed lamella structures with oligopeptide adopting

β-sheets secondary structures (Figure 21a).[60] Molecular modulators such as 4,4'bipyridyl(4Bpy)[60c, 61] and terpyridine (Ter),[62] have also been co-assembled with amyloid peptides to label the C terminus and facilitate the analysis. In these cases, STM images presented linear bright arrays and lamella structures, which could be ascribed to the 4Bpy or Ter moieties and to the assembled polypeptides, respectively (Figure 21b). It was also shown that the arrangement could be modulated by changing the stoichiometry of the oligopeptide and Ter, disrupting the regular lamella structure when a relative ratio 1/5 was used.[62a]

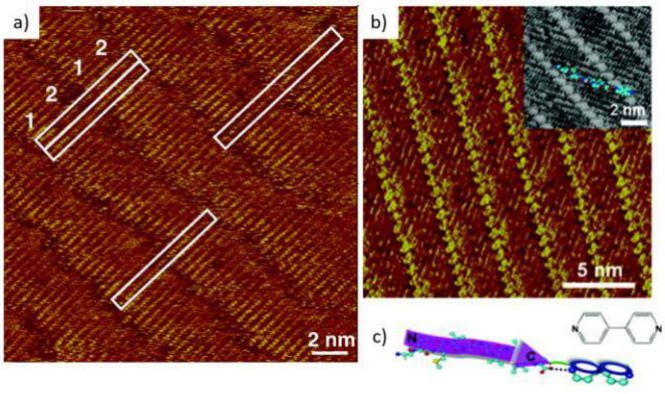

Figure 21. STM images of peptides Aβ42 and modulated Aβ33-42/Bpy. a) STM image of an assembly of Aβ42 on the HOPG surface. 1 and 2 show the brighter and dimmer portions of one β-strand in Aβ42, respectively. The white rectangles indicate occasional long molecular stripes.[60b] b) STM image of Aβ33-42/DP and relative high resolution 3D STM image in the inset. c) The proposed basic building block models for the peptide-modulator complex assemblies for Aβ 33-42/DP.[61a] Adapted from ref [60b] with permission from Elsevier, Copyright 2009 and ref [61a] with permission from American Chemical Society, Copyright 2009

Similar studies concerned the investigation of cell membranes lysis mechanism by antibacterial peptides, which involves the formation of pores.[63] In this context, high-resolution electrochemical scanning

tunneling microscopy (EC-STM) imaging of pores formed in a matrix of phospholipids by the 20-residue antibacterial amphipathic peptide alamethicin (Alm) was reported by *Lipkowski* and co-workers (Figure 22).[63c]

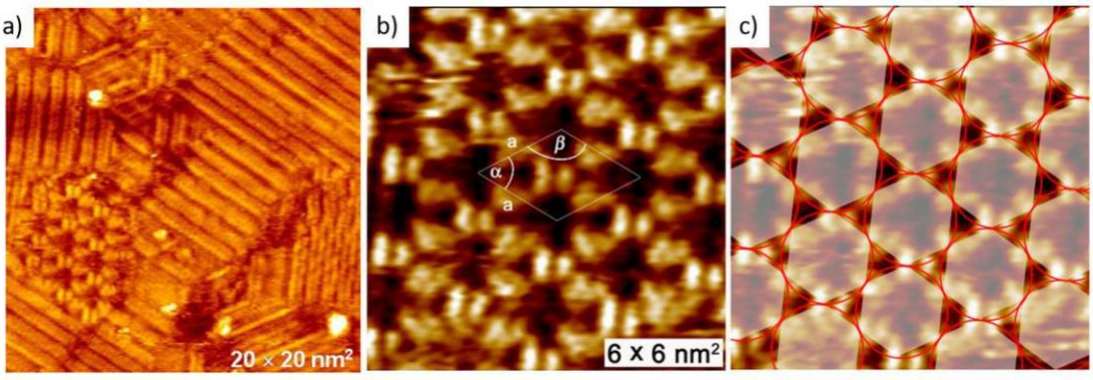

Figure 22. a) EC-STM images of a monolayer of Alm and DMPC/egPG (1:15 molar ratio) deposited on Au(111) surface. b) High-resolution EC-STM image of the flower-like structures, with the superimposed unit cell. c)Scheme superimposed to the EC-STM image showing the channels arrangement.[63c] Adapted from ref [63c].

They incorporated the Alm molecules into a 1/1 mixture of 1,2-dimyristoyl-sn-glycero-3-phosphocholine (DMPC) and egg-PG (egPG), and deposited the obtained monolayer by using the Langmuir–Blodgett technique. Analysis of the monolayer showed segregation of the Alm molecules and phospholipids, with the peptides helical axis orientating parallel to the plane of the monolayer. Subsequent EC-STM analysis of the same monolayer, revealed the presence of two clearly different structures (Figure 22a), one consisting of parallel stripes and the other, embedded on it, forming a "flower-like pattern". The first structure corresponds to a monolayer of close packed phospholipids

while the second is formed by the peptides. High-resolution images of the structure show single Alm molecules arranged with their helical axis perpendicular to the monolayer, which form 2D nanocrystals with a hexagonal lattice and hydrophilic channels with a radius of about 0.5 nm and 1.90 nm apart from each other (Figure 22b-c).

Even though most of the reported studies focused on the self-assembly of amyloid oligopeptides, recently, examples of surfaces supported porous two-dimensional networks built from oligopeptides have started to appear in the literature. *Abb* and co-workers[64] demonstrated that building blocks for two-dimensional self-assembly could be obtained by controlling the amino acids sequence of oligopeptides (Figure 23).

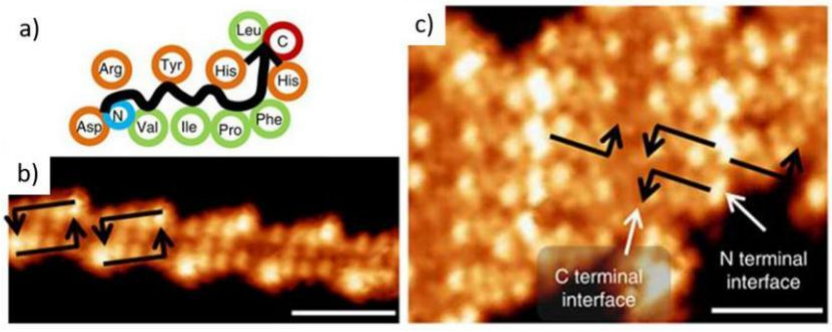

Figure 23. Cartoon of At-I molecular structure and STM images of At-I deposited on Au(111). a) Scheme of the molecular structure of At-I with the polar and nonpolar residues highlighted in orange and green respectively. b) STM image of structure A with black arrows indicating the staggered At-I molecules (scale bar, 4 nm). c) STM image of structure B with black arrows indicating the At-I molecules arranged in stacked assembly and higlight of rows of alternating contrast at the C and N terminal interface (scale bar, 4 nm).[64] Adapted form ref [64] Nature Publishing Group [Open Access], Copyright 2016

They deposited on Au(111) surfaces two oligopeptides, angiotensin I (At-I) and angiotensin II (At-II), by soft-landing electrospray ion

beam deposition (ES-IBD). This technique allows the deposition in UHV conditions of non-volatile oligopeptides avoiding fragmentation. By combining UHV STM imaging, molecular dynamics (MD) and density functional theory DFT calculations, they could evaluate the role of each amino acid in the assembly. This allowed the engineering of long-range ordered hexagonal porous networks by changing the sequence from At-I to At-II. At-I was selected because of the presence of sterically demanding groups that would limit its conformational flexibility when adsorbed on surfaces. MD simulations indicated a L-shape structure of the peptide, with the polar and nonpolar groups of the constituent amino pointing respectively in the opposite sides of the backbone (Figure 23a). By depositing At-I on Au(111) surface and cooling at 40 K, they obtained two different ordered assemblies. The first is composed of regular chains of dimers, where the two components peptides are antiparallel to each other (Figure 23b). The second is a compact array formed of peptides rows, in which they are arranged in parallel stacks along the long side and with opposite orientation in adjacent rows (Figure 23c). The authors attributed these arrangements to the interaction forces established between residues placed nearby the peptide terminals and to the lack of hydrogen bonding formation between neighboring molecules due the steric hindrance caused by their L-shape. In order to form an ordered array, they modified the At-I peptide by removing two amino acids at the C terminal, forming the At-II, which is composed of eight amino acids (Figure 24a). The deposition of At-II

on Au(111) led to the formation of an extended double-walled honeycomb chiral network, with 2.3 nm size pores and a repeating unit of 5.5 nm (Figure 24b). By MD simulations they proposed a model in which the hexagon vertices are formed by the interaction of the C terminal and N terminal on two molecules, where the polar interactions between two adjacent oligopeptides form the double walled structure confining almost completely the nonpolar group at the interior of the pores(Figure 24c).

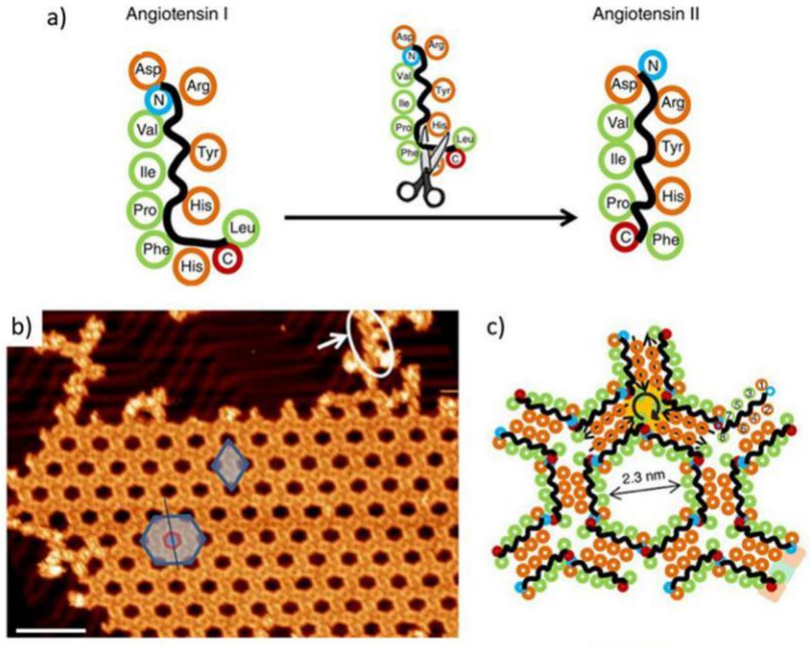

Figure 24. a) Cartoon showing the removal of His9 and Leu10 at the C terminal of At-I to form the linear backbone of At-II on the surface. Polar (orange) and nonpolar (green) residues are segregated at one or other side of the molecule. b) STM image of a large, honeycomb network of At-II on Au(111) surface. The diamond indicates the unit cell, the hexagon highlights the chirality of the network showing the tilting of the hexagonal pore (red) anticlockwise by 6° with respect to the hexagonal superstructure (blue), (scale bar, 15 nm). c) The cartoon of the arrangement of the At-II molecules in accordance to MD simulations demonstrating the nonpolar (green) decorated pore and the polar residues (orange) positioned within the walls of the nanostructure. A circular arrow indicates the chiral vertex.[64] Adapted from ref [64], Nature Publishing Group [Open Access], Copyright 2016

By using a different approach, the group of Wennemers[65] reported the formation of porous hexagonal structures with a "Kagome" lattice, extending over more than one micrometre in size (Figure 25b), from the self-assembly of a rigid oligoproline peptide functionalized with two perylenemonoimide (PMI) chromophores positioned at 18 Å from each other (**1**) (Figure 25a).

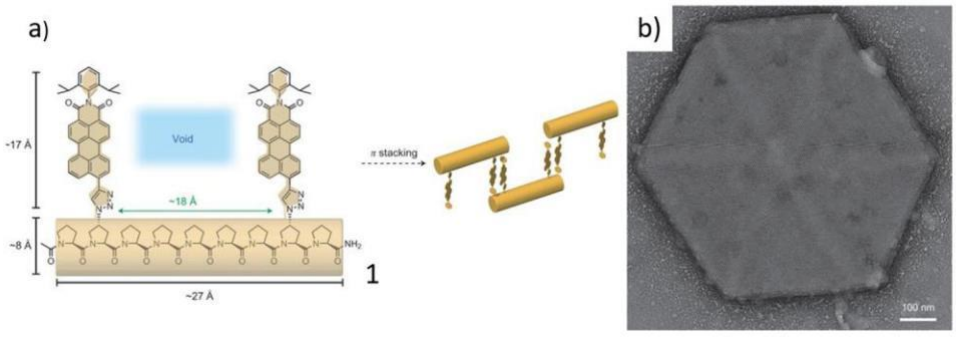

Figure 25. a) Structure of PMI functionalized oligoproline **1**.b) TEM micrograph of micrometre-sized structure of self-assembled **1**.[65] Adapted from ref [65] by permission from Springer Nature, Copyright 2017

The self-assembly into extended triaxial supramolecular weaves is dominated by π-π interactions between the perylenemonoimide substituents. The units form supramolecular organic threads with alternating voids at regular distances. These consist of crossing point that trough CH-π interactions with other threads form the woven structure (Figure 26). AFM, TEM and selected area electron diffraction (SADPs) analyses showed pores of 3 nm in diameter and a repeating unit of 5.5 nm (Figure 26a). This corresponds to double the size of **1** and it is consistent with the self-assembly head to tail of the molecules.

More detailed information about the organisation of the molecules in the assembly could be obtained by grazing incidence wide-angle X-ray scattering, which further confirmed the proposed woven structure.

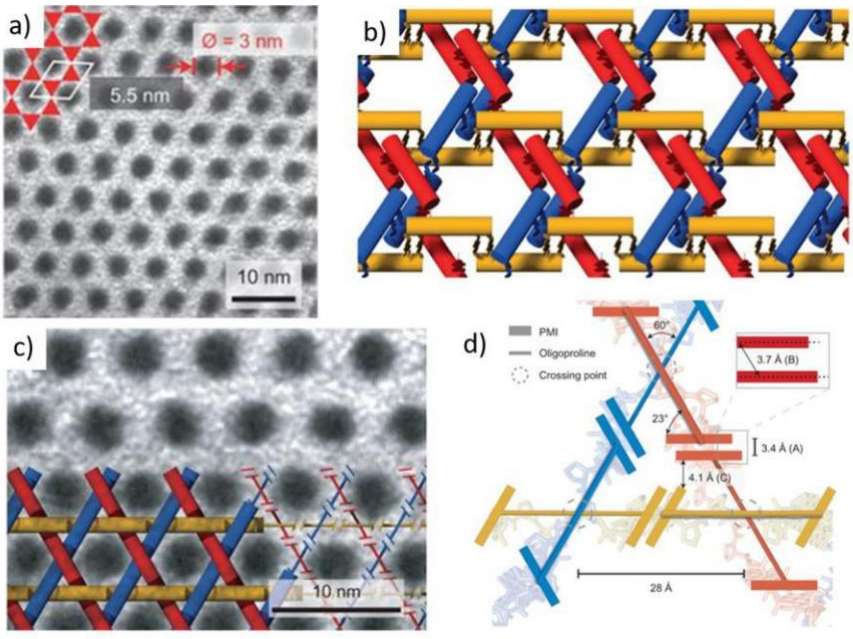

Figure 26. a) TEM micrograph at higher magnification of self-assembled **1** (the white rhombus shows the unit cell, the red triangles indicate the trihexagonal geometry and the red arrows the pore diameter. b) Cartoon of the triaxial weave formed by interdigitation of the three supramolecular threads. c) Representation of the molecular weave superimposed on the TEM micrograph with the right side showing the arrangement of the chromophores within the structure. d) Top view of the triangular connecting points showing the chromophores (thick lines) arrangement and their π stacking distances as calculated by the GIWAXS data. The oligoproline scaffolds are represented by the thin lines.[65] Adapted from ref [65] by permission from Springer Nature, Copyright 2017

The hexagonal pores in the structures were used to build and localise iridium nanoparticles (Ir-NPs). In a similar fashion, a stiff proline rich peptide containing two cysteine amino acids at specific positions was used to localize electron spins by attaching various spin labels to the cysteine residues, producing a molecular qubit-based network.[66]

Proteins-based networks. Ordered two-dimensional patterns formed by proteins have also been used to organise biotinylated compounds,[67] nanoparticles, and quantum dots.[68] S-layers, which are two-dimensional porous crystalline bacterial cell membranes, consisting of protein or glycoprotein,[69] have been used for this purpose[68c, 70] and assembled on various surfaces to fabricate biosensors.[71] An example of self-assembly of Au NPs into hexagonal lattices templated by a S-layer protein, the hexagonally packed intermediate (HPI) of *Deinococcus radiodurans*, was described by *Mann* and co-workers.[68b] The hexagonal HPI structure is formed by hexameric units, which form a cone with a positively charged central 2 nm wide channel.

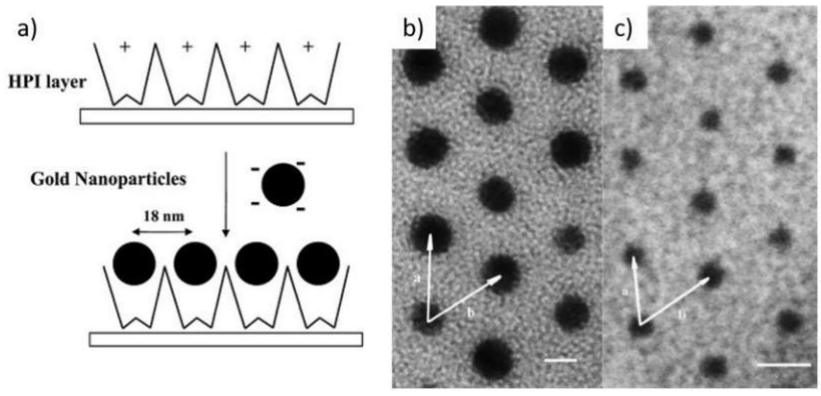

Figure 27. a) Schematic representation of Au NPs self-assembly directed by S-layer templates. b) and c) High resolution TEM images of hexagonal arrays of Au nanoparticles with mean sizes of approximately 8nm and 5 nm respectively, on self-assembled HPI layers. Vectors a and b show the centre-to-centre average distance of 18 nm (scale bars are 7 and 10 nm, respectively).[68b] Adapted from ref [68b] with permission from WILEY‐VCH Verlag GmbH & Co. KGaA, Weinheim, Copyright 2001

Micrometre-sized arrays of regularly arranged (18 nm centre to centre) Au NPs could be obtained by exposing the hydrophilic surface of self-assembled HPI layers, which had been previously deposited onto

hydrophobic TEM grids, to negatively charged monodisperse nanoparticles colloids (Figure 27).

S-layers were also used to form fusion proteins with streptavidin, which showed the streptavidin organised with defined spacing (Figure 28a). These were able to bind biotin and biotinylated compounds, which could be arranged in regular patterns on surfaces such as liposomes, silicon wafers and cell wall fragments (Figure 28b).[67a]

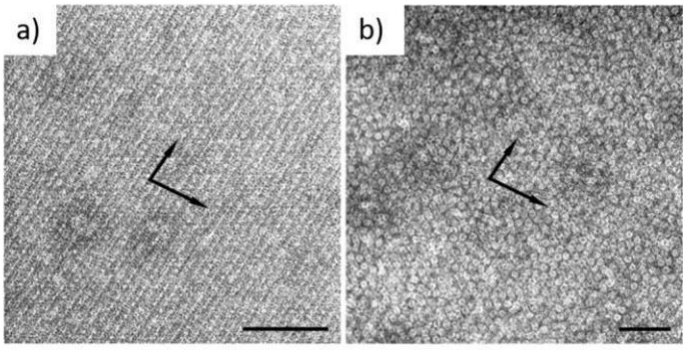

Figure 28. TEM images of a) Fusion protein BS1(S1)$_3$ S-layer on cell wall fragments and b) S-layer with biotinylated ferritin. The arrows indicate the base vectors of the oblique p1 lattice (scale bars = 100 nm.[67a] Adapted from ref [67a] with permission from National Academy of Sciences, U.S.A., Copyright 2002

Similarly , *McMillan* and co-workers[68a] reported the use of genetically modified chaperonins for the formation of ordered arrays of gold nanoparticles or CdSe–ZnS semiconductor quantum dots (Figure 29c-d). These proteins were assembled from genetically modified subunits containing thiol functionalised 3 nm and 9 nm apical pores and formed up to 20 micrometres large two-dimensional crystals. The assemblies were visualised by TEM (Figure 29). Chaperonins are heat shock proteins (HSP60) composed of 14, 16 or 18 60-kDa subunits, arranged to form two stacked rings, inadvertently that can form two dimensional crystals.[72]

The two classes of genetically modified proteins were obtained by the modification of the beta subunit of the octadecameric chaperonin from *Sulfolobus Shibatae*. In both cases, a non-reactive alanine was substituted to the single native cysteine residue in the subunit and cysteine residues were inserted in various solvent-exposed sites so that they could provide binding sites for metals such as gold and zinc. For one variant, the cysteine was introduced close to the tip of a 28 amino acids loop on the apical domain of the subunit, which in the assembled chaperonin would form a ring with a diameter of approximately 3 nm of reactive thiols that could bind the nanoparticles.

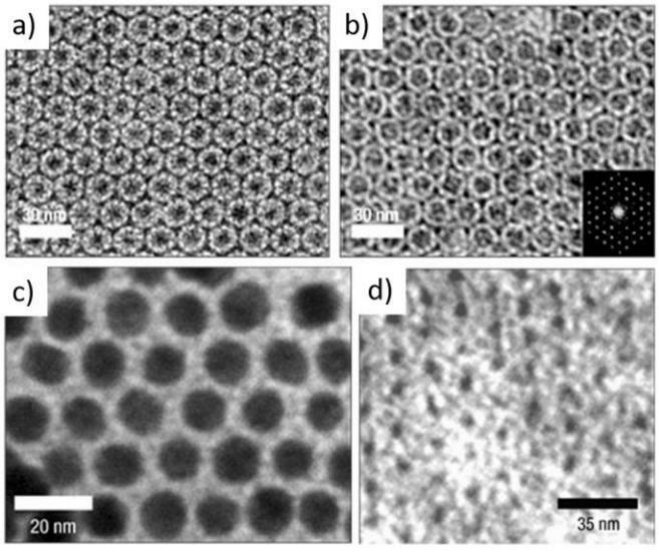

Figure 29. TEM images of a negatively stained 2D crystal a) of the beta chaperonin mutant with cysteine at the apical position of the 3 nm wide pores, b) of the chaperonin mutant with 9 nm wide pore, c) of an ordered area of 9 nm pore chaperonin with bound 10 nm Au NPs. d) High magnification TEM image of an ordered area of 3 nm pore chaperonin with bound 4.5 nm luminescent CdSe–ZnS QDs.[68a] Adapted from ref [68a] by permission from Springer Nature, Copyright 2002

In the other variant, the 28 amino acid loop was removed and the

cysteine placed in the apical site, so that the deriving chaperonin had an approximately 9 nm wide ring of reactive thiols.

In a complementary work, *Yamashita* and co-workers[73] reported the use of self-assembled iron-oxide loaded ferritin two-dimensional crystals to obtain an ordered pattern of iron-oxide nanoparticles onto a hydrophobic Si surface. The regular proteins array was formed at an air-water interface and then transferred onto the Si surface. The proteins were removed by one-hour heat treatment at 500 ^{o}C under N_2 leaving the iron cores pattern on the surface (Figure 30).

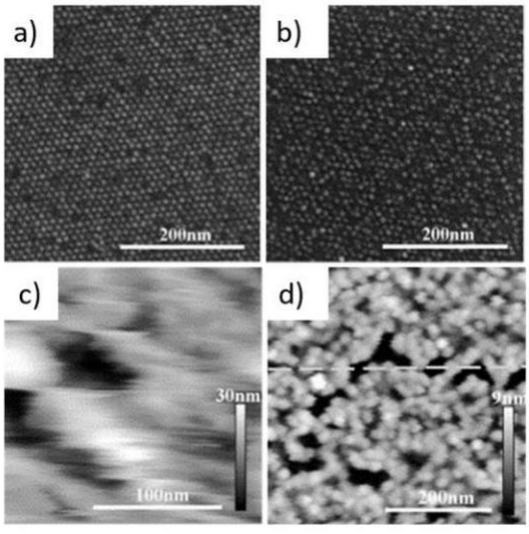

Figure 30. a-b) H-SEM images and c-d) AFM images of arrays of the ferritin molecules before and after heat-treatment under nitrogen at 500 ^{o}C for 1 h, respectively. In the SEM images the array of iron oxide cores can be observed up to the 500 ^{o}C heat-treatment. In the AFM images the inset of the gray vertical bar shows the height scale. The AFM image before heat-treatment was very obscure and individual molecules could not be observed. After heat-treatment clearer images of distinct cores could be detected.[73] Adapted from ref [73] with permission from Elsevier, Copyright 2001

More recently, the group of *Wang*[74] described the formation of regular nanoparticles two-dimensional arrays by employing genetically modified

cylinder-shaped tobacco mosaic virus coat protein (TMV disks), which is formed by 34 TMV coat protein subunits, arranged to form a cylindric structure with a central pore of 4 nm. They modified the TMV disk by substituting a threonine residue, which points toward the central pore, with a cysteine that could form disulphide bonds between adjacent constituent units (T103C-TMV). Furthermore, they introduced four histidine fragments at the C-terminal on the periphery of the disk (T103C-TMV-4his, Figure 31a).

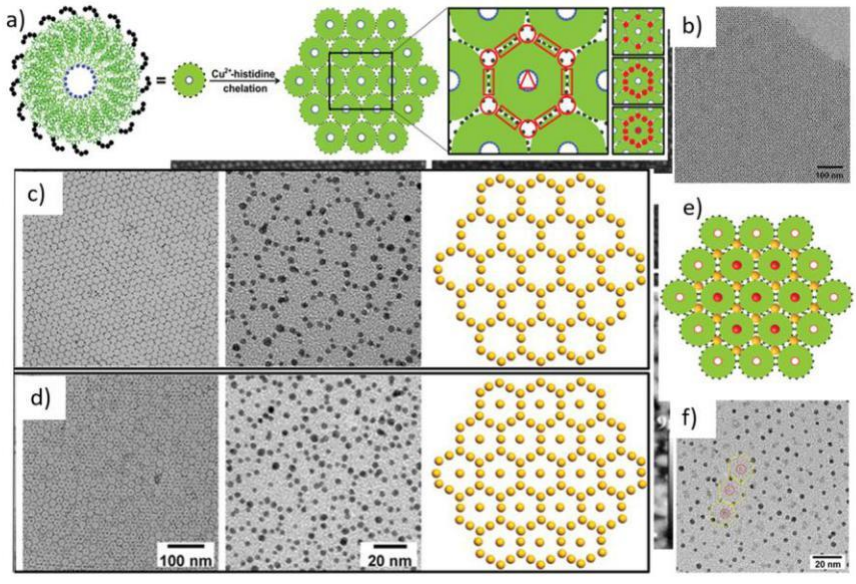

Figure 31. a) Scheme of assembly of T103C-TMV-4his disks into ordered monolayer via coordinative interactions with Cu_{2+}. The circle, rectangle, and triangle represent three different functional sites for binding nanoparticles in the monolayer. b)TEM image of TMV array. c–d) TEM images and relative schemes of two different 2D AuNP patterns. e-f) Scheme and TEM image of 2D binary nanoparticles arrays assembled on the T103C-TMV-4his monolayer sheet consisting of six AuNPs at the vertexes and a CdSe@ZnS QD at the centre.[74] Adapted from ref [68b] with permission from WILEY‐VCH Verlag GmbH & Co. KGaA, Weinheim, Copyright 2019

Both the cysteine and histidine residues were able to bind gold nanoparticles. They exploited the coordination chemistry to arrange the

modified T103C-TMV-4his disks into ordered honeycomb arrays on $Cu(OH)_2$ nanowire-haired mesh(see mesh TEM analysis in Figure 31b).

By controlling the ionic strength and pH of the solution, which influenced the affinity of the nanoparticles to the functional sites, they could obtain three different AuNPs patterns, up to tens of micrometres in size (Figure 31c-d). The dual functionality provided by the insertion of cysteine and histidine in the TMV disks allowed the construction of regular two-dimensional patterns containing two different kind of nanoparticles. For instance, one of these mixed regular arrays was obtained by introducing first the AuNPs, which bound to the histidine residues on the six vertices of the disks on the honeycomb structure, and then by activating the cysteine residue with tris(2-carboxyethyl)phosphine to form thiol groups, the latter directing the CdSe@ZnS QDs into the central pores of the disk (Figure 31e-f).

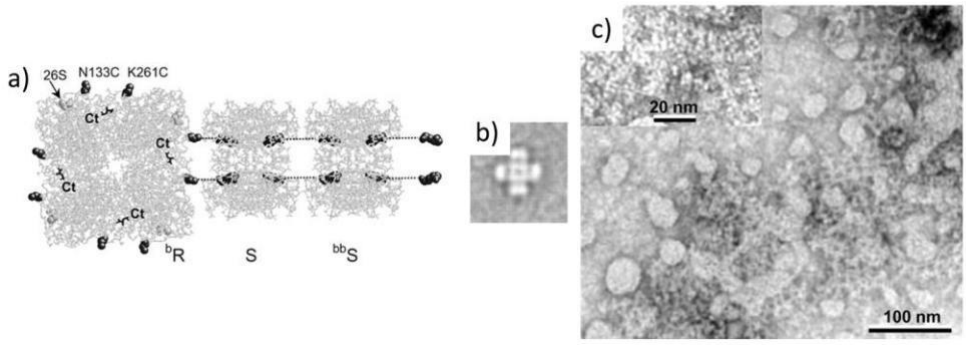

Figure 32. a) Block construction extended with a biotinylated streptavidin. b) Block $_bRS_4$. c) Negatively stained TEM image of the networks formed by self-assembly of blocks $_bR$ and $_bRS_4$ at a lipid monolayer. The lattices have sizes of 200 nm by 200 nm but present irregularities.[75] Adapted from ref [75] with permission from The American Association for the Advancement of Science, Copyright 2003

In a different approach, *Ringler* and *Shultz*[75] designed and built proteins self-assembled networks on lipid monolayer, using L-rhamnulose-1-phosphate aldolase (RhuA) and streptavidin as building blocks (Figure 32).

RhuA is a tetramer with a tetragonal shape of 7 nm by 7 nm by 5 nm size. Streptavidin (S) has a brick-shape with dimensions of 6 nm by 5 nm by 4 nm and two biotin-binding sites on each of the two 6-nm-by-4-nm faces, which were used for the self-assembly. To direct the self-assembly on the lipid monolayer, a His6 tag was added to C termini of each monomeric unit protruding from the top face of RhuA. This was further modified to bind eight biotins in designed positions to form the building block ^{b}R, which could interact with the biotin-binding sites of streptavidin to build the network (Figure 32a-b). They formed the building block $^{b}RS_4$ and then mixed it in solution with an equimolar amount of ^{b}R and obtained planar networks of 50nm by 50 nm in size with a ^{b}R intermolecular distance of 13 nm, consistent with the dimension of the streptavidin spacer. Larger networks extending more than 200 nm could be obtained by incubating the solution on a lipid monolayer (Figure 32c).

Recently, *Sinclair* and co-workers[76] described a strategy for the design of proteins two-dimensional lattices based on the genetic fusion of proteins subunits with matching rotational symmetry. They named the deriving ordered structures “crysalins” (Figure 33).

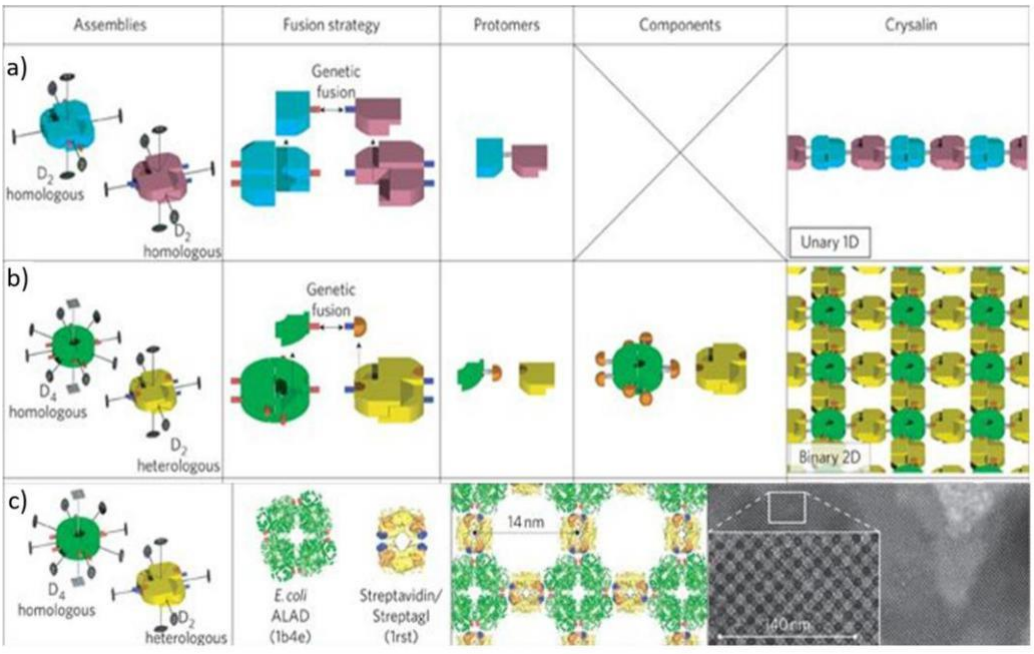

Figure 33. Design of crysalins. N- and C-termini of fusion peptide chains are in blue and orange cylinders, respectively. Rotational two-, three- and fourfold symmetry axes in the original assemblies are represented by lines and corresponding IUCr symbols. a) Scheme of a unary 1D crysalin formed by fusion along a twofold axis. Generated by a protomer obtained by homologous assemblies b) A binary 2D crysalin formed by one fusion between homologous D4 and heterologous D2 assemblies. c) A 2D crysalin lattice containing ALAD and streptavidin/Streptag I assemblies with corresponding TEM image.[76] Adapted from ref [76] with permission from Springer Nature, Copyright 2011

They obtained what they call "protomers" from the genetic fusion of two peptide chains from different proteins. When "Protomers" were obtained by the fusion of a unit from a homologous assembly and one from a heterologous assembly (a protein composed of different types of peptide chains), they could form "components" that could be mixed to obtain binary "crysalins" (Figure 33b-c). Two-dimensional lattice could be obtained by the fusion of the Streptag with high-symmetry assemblies, which were then interconnected along their twofold axes with streptavidin (Figure 33c).

Role of the solid support.

While the formation of non-covalent arrays of small molecules on solid surfaces either at the solid-liquid or at the solid-vacuum interface is greatly dictated by both intermolecular and molecule-surface interactions,[9, 15d, 16a] the self-assembly of biomacromolecules generally takes place in solution and the resulting array are then transferred onto surfaces (i.e., mica) for characterization.[31-32, 39-40, 42, 45, 49, 59] Nevertheless, in some cases it has been shown that if the self-assembly of DNA is performed in the presence of mica, it favours the adsorption of the arrays as it forms, avoiding destructive shear forces associated with the deposition process onto surfaces. Thee forces often lead to fragmentation of the fragile array.[41, 44] In this case, single DNA tiles are usually obtained in solution and incubated with the mica support at a specific temperature, which will trigger the network formation.[41] Furthermore, the interactions with the solid support promote the formation of extended two-dimensional networks from more flexible tiles, which would not be possible to be obtained in solution.[41, 55-56] It has been also observed that mica-assisted self-assembly promotes the formation of extended 2D arrays from two single-duplex DNA helices "T-shaped" junction tiles.[55-56] In another work, the authors described that mica-supported zwitterionic lipid bilayer in the presence of divalent cations, such as Mg^{2+},[46] or both divalent and monovalent cations, such Mg^{2+} and Na^{+},[47, 52] assists the self-assembly of origami tiles into 2D-ordered networks, by electrostatically adsorbing them

and, at the same time, allowing enough mobility for the formation of regular arrays. Similarly, SiO2 surfaces can be lithographically patterned and hydrolysed to electrostatically attract DNA origami tiles in the presence of buffer solutions containing Mg^{2+} ions and lead to their organisation in regular 2D-arrays. The tiles can be afterwards covalently bound to the surfaces by crosslinking reagents.[50] As for DNA, most of the peptides- and proteins-based porous two-dimensional networks are obtained in solution and then transferred into solid supports for analysis or for engineering functional devices.[63c, 65, 67a, However, surfaces such as Au have been used in combination with soft-landing electrospray ion beam deposition to directly form supported two-dimensional structures from oligopeptides.[64] Furthermore, coordination chemistry has been used to form ordered porous arrays from proteins. For instance, modified tobacco mosaic virus could be organised into ordered honeycomb arrays through coordination to $Cu(OH)_2$ nanowire-haired mesh.[74]

The self-assembly of such biomacromolecular structures that can selectively and spontaneously lead to the formation of ordered domains and networks on surfaces is a very promising approach for the construction of organic materials for nanotechnological application, because, in principle, it permits the controlled, large amplitude formation and positioning of molecules with respect to others. Therefore, if one wants to explore routes leading to the integration of the self-assembled networks into functional devices, the

immobilization on solid surfaces is very important to probe the very local properties, functions, and accessibility of the array. Depending on the applications, i.e. sensing, lithography, and templated synthesis, one should also explore semiconducting or metallic surfaces and study their electronic or optical coupling with the biomolecular array for a specific application.

Conclusions.

Two-dimensional porous networks on surfaces constitute an active field of research as they could be used to template the structure of functional materials with potential applications in nanotechnology, nanoelectronics, sensing and catalysis. For instance, they can be used to tailor the organisation of functional guests or anchored molecular species onto a surface and build complex materials. The rapid development of imaging techniques (scanning probe and electron-based microscopies), which allow structural characterisation with nanometric resolution and help to elucidate how these networks form, have greatly contributed to the progress of this field. While early works took advantage of the recognition properties of small organic molecules to build extended 2D porous networks both at the solid-vacuum and solid-liquid interfaces, the field has now moved toward the use of programmed macromolecules that can form robust architectures directly from aqueous solutions. It is with the aim of highlighting these developments in the field that this review describes the current bottom-up approaches for

the fabrication of porous nanostructures on surfaces using biomolecules encoding specific recognition and self-assembly properties. In particular, in this report we focused on the use of nucleic acid and polypeptide scaffolds. Programming of their self-assembly and functional properties can be obtained through specific sequencing of their nucleobase and amino acid constituents, respectively. This has led to the engineering of a series of architectures of predictable structures, with tailored pore size and shape. Through the introduction of lateral sticky sides, these 2D nanostructures could be used to subsequently pattern functional, guest molecules into ordered arrays at the nanoscale level. Thanks to their biocompatibility, water solubility and easy chemical functionalization, these biomacromolecules open to new opportunities for designing functional architectures for biological and biomedical applications, creeping closer to the objective of engineering multifunctional devices.

References.

[1] H. Wang, X. Ji, Z. Li and F. Huang, *Adv. Mater.* **2017**, *29*, 1606117.

[2] a) D. Bonifazi, S. Mohnani and A. Llanes-Pallas, *Chem. Eur. J.* **2009**, *15*, 7004-7025; b) R. Tian, D. Yan, C. Li, S. Xu, R. Liang, L. Guo, M. Wei, D. G. Evans and X. Duan, *Nanoscale* **2016**, *8*, 9815-9821; c) G. P. Acuna, F. M. Möller, P. Holzmeister, S. Beater, B. Lalkens and P. Tinnefeld, *Science* **2012**, *338*, 506-510.

[3] a) Y.-S. Wei, M. Zhang, P.-Q. Liao, R.-B. Lin, T.-Y. Li, G. Shao, J.-P. Zhang and X.-M. Chen, *Nat. Commun.* **2015**, *6*, 8348; b) H. Zhao, S. Sen, T. Udayabhaskararao, M. Sawczyk, K. Kučanda, D. Manna, P. K. Kundu, J.-W. Lee, P. Král and R. Klajn, *Nat. Nanotechnol.* **2015**, *11*, 82-88; c) S. L. Anderson, P. G. Boyd, A. Gładysiak, T. N. Nguyen, R. G. Palgrave, D. Kubicki, L. Emsley, D. Bradshaw, M. J. Rosseinsky, B. Smit and K. C. Stylianou, *Nat. Commun.* **2019**, *10*, 1612; d) J. M. Thomas and R. Raja, *Acc. Chem. Res.* **2008**, *41*, 708-720.

[4] a) B. Hulsken, R. Van Hameren, J. W. Gerritsen, T. Khoury, P. Thordarson, M. J. Crossley, A. E. Rowan, R. J. M. Nolte, J. A. A. W. Elemans and S. Speller, *Nat. Nanotechnol.* **2007**, *2*, 285-289; b) X. Zhang, Q. Zeng and C. Wang, *RSC Adv.* **2013**, *3*, 11351-11366.

[5] C. Tian, H. Kim, W. Sun, Y. Kim, P. Yin and H. Liu, *ACS Nano* **2017**, *11*, 227-238.

[6] With the term "programmed", here we referred to biomacromolecules that have been prepared with encoded structural information, which determines their self-assembly behavior and dictate the formation of the macroscopic assembly.

[7] For the definition of "self-assembly" we refer to the paper by G. M. Whitesides and B. Grzybowski, *Science* **2002**, 295, 2418-2421. DOI: 10.1126/science.1070821

[8] a) P. Samorì, *Chem. Soc. Rev.* **2005**, *34*, 551-561; b) P. Samorì, *J. Mater. Chem.* **2004**, *14*, 1353-1366; c) M. Stöhr in *Scanning Tunneling Microscopy, in Supramolecular Chemistry: From Molecules to Nanomaterials*, *Vol. 2* John Wiley & Sons, Ltd, **2012**, pp. 647-658

[9] T. Kudernac, S. Lei, J. A. A. W. Elemans and S. De Feyter, *Chem. Soc. Rev.* **2009**, *38*, 402-421.

[10] J.-M. Lehn, *Science* **2002**, *295*, 2400-2403.

[11] a) S. Griessl, M. Lackinger, M. Edelwirth, M. Hietschold and W. M. Heckl, *Single Mol.* **2002**, *3*, 25-31; b) A. Dmitriev, N. Lin, J. Weckesser, J. V. Barth and K. Kern, *J. Phys. Chem. B* **2002**, *106*, 6907-6912; c) J. Lu, S.-b. Lei, Q.-d. Zeng, S.-z. Kang, C. Wang, L.-j. Wan and C.-l. Bai, *J. Phys. Chem. B* **2004**, *108*, 5161-5165; d) J. A. Theobald,

N. S. Oxtoby, M. A. Phillips, N. R. Champness and P. H. Beton, *Nature* **2003**, *424*, 1029-1031; e) M. Lackinger, S. Griessl, T. Markert, F. Jamitzky and W. M. Heckl, *J. Phys. Chem. B* **2004**, *108*, 13652-13655; f) L. Kampschulte, S. Griessl, W. M. Heckl and M. Lackinger, *J. Phys. Chem. B* **2005**, *109*, 14074-14078; g) L. Kampschulte, M. Lackinger, A.-K. Maier, R. S. K. Kishore, S. Griessl, M. Schmittel and W. M. Heckl, *J. Phys. Chem. B* **2006**, *110*, 10829-10836; h) L. M. A. Perdigão, N. R. Champness and P. H. Beton, *Chem. Commun.* **2006**, 538-540; i) D. Payer, A. Comisso, A. Dmitriev, T. Strunskus, N. Lin, C. Wöll, A. DeVita, J. V. Barth and K. Kern, *Chem. Eur. J.* **2007**, *13*, 3900-3906; j) W. Xu, M. Dong, H. Gersen, E. Rauls, S. Vázquez-Campos, M. Crego-Calama, D. N. Reinhoudt, I. Stensgaard, E. Laegsgaard and T. R. Linderoth, *Small* **2007**, *3*, 854-858; k) J. A. Gardener, O. Y. Shvarova, G. A. D. Briggs and M. R. Castell, *J. Phys. Chem. C* **2010**, *114*, 5859-5866; l) W. Xu, J. g. Wang, M. F. Jacobsen, M. Mura, M. Yu, R. E. Kelly, Q. q. Meng, E. Lægsgaard, I. Stensgaard and T. R. Linderoth, *Angew. Chem. Int. Ed.* **2010**, *49*, 9373-9377; m) H. Liang, W. Sun, X. Jin, H. Li, J. Li, X. Hu, B. K. Teo

and K. Wu, *Angew. Chem. Int. Ed.* **2011**, *50*, 7562-7566; n) A. Ciesielski, S. Haar, G. Paragi, Z. Kupihár, Z. Kele, S. Masiero, C. F. Guerra, F. M. Bickelhaupt, G. P. Spada and L. Kovács, *Phys. Chem. Chem. Phys.* **2013**, *15*, 12442-12446; o) H. Dai, W. Yi, K. Deng, H. Wang and Q. Zeng, *ACS Appl. Mater. Interfaces* **2016**, *8*, 21095-21100; p) X. Peng, Y. Geng, M. Zhang, F. Cheng, L. Cheng, K. Deng and Q. Zeng, *Nano Res.* **2019**, *12*, 537-542; q) L. Perdigao, E. Perkins, J. Ma, P. Staniec, B. Rogers, N. Champness and P. Beton, *J. Phys. Chem. B* **2006**, *110*, 12539-12542; r) J. Theobald, N. Oxtoby, N. Champness, P. Beton and T. Dennis, *Langmuir* **2005**, *21*, 2038-2041.

[12] a) N. Lin, A. Dmitriev, J. Weckesser, J. V. Barth and K. Kern, *Angew. Chem. Int. Ed.* **2002**, *41*, 4779-4783; b) H. Spillmann, A. Dmitriev, N. Lin, P. Messina, J. V. Barth and K. Kern, *J. Am. Chem. Soc.* **2003**, *125*, 10725-10728; c) A. Dmitriev, H. Spillmann, N. Lin, J. V. Barth and K. Kern, *Angew. Chem. Int. Ed.* **2003**, *42*, 2670-2673; d) S. Stepanow, M. Lingenfelder, A. Dmitriev, H. Spillmann, E. Delvigne, N. Lin, X. Deng, C. Cai, J. V. Barth and K. Kern, *Nat. Mater.* **2004**, *3*, 229-233; e) N. Lin, S. Stepanow, F. Vidal, J. V. Barth and K. Kern, *Chem. Commun.* **2005**, 1681-1683; f) S. Stepanow, N. Lin, J. V. Barth and K. Kern, *J. Phys. Chem. B* **2006**, *110*, 23472-23477; g) S. Stepanow, N. Lin, J. V. Barth and K. Kern, *Chem. Commun.* **2006**, 2153-2155; h) S. Stepanow, N. Lin, D. Payer, U. Schlickum, F. Klappenberger, G. Zoppellaro, M. Ruben, H. Brune, J. V. Barth and K. Kern, *Angew. Chem. Int. Ed.* **2007**, *46*, 710-713; i) A. Langner, S. L. Tait, N. Lin, C. Rajadurai, M. Ruben and K. Kern, *Proc. Natl. Acad. Sci.* **2007**, *104*, 17927-17930; j) S. L. Tait, A.

Langner, N. Lin, R. Chandrasekar, O. Fuhr, M. Ruben and K. Kern, *ChemPhysChem* **2008**, *9*, 2495-2499; k) S. Vijayaraghavan, D. Ecija, W. Auwärter, S. Joshi, K. Seufert, M. Drach, D. Nieckarz, P. Szabelski, C. Aurisicchio and D. Bonifazi, *Chem. Eur. J.* **2013**, *19*, 14143-14150; l) T. Umbach, M. Bernien, C. F. Hermanns, L. Sun, H. Mohrmann, K. Hermann, A. Krüger, N. Krane, Z. Yang and F. Nickel, *Phys. Rev. B* **2014**, *89*, 235409; m) M. Matena, J. Björk, M. Wahl, T. -L. Lee, J. Zegenhagen, L. H. Gade, T. A. Jung, M. Persson and M. Stöhr, *Phys. Rev. B* **2014**, *90*, 125408-125415; n) B. Cirera, L. Đorđević, R. Otero, J. M. Gallego, D. Bonifazi, R. Miranda and D. Ecija, *Chem. Commun.* **2016**, *52*, 11227-11230; o) L. Dong, Z. A. Gao and N. Lin, *Prog. Surf. Sci.* **2016**, *91*, 101-135; p) U. Schlickum, F. Klappenberger, R. Decker, G. Zoppellaro, S. Klyatskaya, M. Ruben, K. Kern, H. Brune and J. Barth, *J. Phys. Chem. C* **2010**, *114*, 15602-15606; q) U. Schlickum, R. Decker, F. Klappenberger, G. Zoppellaro, S. Klyatskaya, M. Ruben, I. Silanes, A. Arnau, K. Kern and H. Brune, *Nano Lett.* **2007**, 7, 3813-3817; r) J. I. Urgel, M. Schwarz, M. Garnica, D. Stassen, D. Bonifazi, D. Ecija, J. V. Barth and W. Auwärter *J. Am. Chem. Soc.* **2015**, *137,* 2420-2423; s) J. I. Urgel, D. Ecija, W. Auwärter, D. Stassen, D. Bonifazi and J. V. Barth *Angew. Chem. Int. Ed.* **2015**, *54*, 6163-6167; t) S. Kervyn, N. Kalashnyk, M. Riello, B. Moreton, J. Tasseroul, J. Wouters, T. S. Jones, A. De Vita, G. Costantini and D. Bonifazi *Angew. Chem. Int. Ed.* **2013**, 52, 7410-7412.

[13] a) H. Spillmann, A. Kiebele, M. Stöhr, T. A. Jung, D. Bonifazi, F. Cheng and F. Diederich, *Adv. Mater.* **2006**, *18*, 275-279; b) D. Bonifazi,

A. Kiebele, M. Stöhr, F. Cheng, T. Jung, F. Diederich and H. Spillmann, *Adv. Funct. Mater.* **2007**, *17*, 1051-1062.

[14] a) S. Furukawa, H. Uji-i, K. Tahara, T. Ichikawa, M. Sonoda, F. C. De Schryver, Y. Tobe and S. De Feyter, *J. Am. Chem. Soc.* **2006**, *128*, 3502-3503; b) S. Lei, K. Tahara, F. C. De Schryver, M. Van der Auweraer, Y. Tobe and S. De Feyter, *Angew. Chem. Int. Ed.* **2008**, *47*, 2964-2968; c) S. Lei, K. Tahara, X. Feng, S. Furukawa, F. C. De Schryver, K. Müllen, Y. Tobe and S. De Feyter, *J. Am. Chem. Soc.* **2008**, *130*, 7119-7129; d) G. Schull, L. Douillard, C. Fiorini-Debuisschert, F. Charra, F. Mathevet, D. Kreher and A.-J. Attias, *Nano Lett.* **2006**, *6*, 1360-1363; e) K. Tahara, K. Katayama, M. O. Blunt, K. Iritani, S. De Feyter and Y. Tobe, *ACS Nano* **2014**, *8*, 8683-8694; f) E. Ghijsens, O. Ivasenko, K. Tahara, H. Yamaga, S. Itano, T. Balandina, Y. Tobe and S. De Feyter, *ACS Nano* **2013**, *7*, 8031-8042; g) K. Tahara, J. Adisoejoso, K. Inukai, S. Lei, A. Noguchi, B. Li, W. Vanderlinden, S. De Feyter and Y. Tobe, *Chem. Commun.* **2014**, *50*, 2831-2833; h) B. Li, K. Tahara, J. Adisoejoso, W. Vanderlinden, K. S. Mali, S. De Gendt, Y. Tobe and S. De Feyter, *ACS Nano* **2013**, *7*, 10764-10772; i) M. O. Blunt, J. Adisoejoso, K. Tahara, K. Katayama, M. Van der Auweraer, Y. Tobe and S. De Feyter, *J. Am. Chem. Soc.* **2013**, *135*, 12068-12075; j) K. Tahara, K. Nakatani, K. Iritani, S. De Feyter and Y. Tobe, *ACS Nano* **2016**, *10*, 2113-2120; k) K. Tahara, S. Lei, D. Mössinger, H. Kozuma, K. Inukai, M. Van der Auweraer, F. C. De Schryver, S. Höger, Y. Tobe and S. De Feyter, *Chem. Commun.* **2008**, 3897-3899; l) K. Tahara, S. Furukawa, H. Uji-i, T. Uchino, T. Ichikawa, J. Zhang, W. Mamdouh, M. Sonoda, F. C. De Schryver and S. De Feyter, *J.*

Am. Chem. Soc. **2006**, *128*, 16613-16625; m) S. Furukawa, K. Tahara, F. C. De Schryver, M. Van der Auweraer, Y. Tobe and S. De Feyter, *Angew. Chem. Int. Ed.* **2007**, *46*, 2831-2834.

[15] a) K.-H. Chung, H. Kim, W. J. Jang, J. K. Yoon, S.-J. Kahng, J. Lee and S. Han, *J. Phys. Chem. C* **2013**, *117*, 302-306; b) Q.-N. Zheng, X.-H. Liu, T. Chen, H.-J. Yan, T. Cook, D. Wang, P. J. Stang and L.-J. Wan, *J. Am. Chem. Soc.* **2015**, *137*, 6128-6131; c) A. Mukherjee, J. Teyssandier, G. Hennrich, S. De Feyter and K. S. Mali, *Chem. Sci.* **2017**, *8*, 3759-3769; d) D. P. Goronzy, M. Ebrahimi, F. Rosei, Arramel, Y. Fang, S. De Feyter, S. L. Tait, C. Wang, P. H. Beton, A. T. S. Wee, P. S. Weiss and D. F. Perepichka, *ACS Nano* **2018**, *12*, 7445-7481; e) L. Xing, W. Jiang, Z. Huang, J. Liu, H. Song, W. Zhao, J. Dai, H. Zhu, Z. Wang, P. S. Weiss and K. Wu, *Chem. Mater.* **2019**, *31*, 3041-3048.

[16] a) A. G. Slater, P. H. Beton and N. R. Champness, *Chem. Sci.* **2011**, *2*, 1440-1448; b) J. Teyssandier, S. D. Feyter and K. S. Mali, *Chem. Commun.* **2016**, *52*, 11465-11487; c) X. Bouju, C. Mattioli, G. Franc, A. Pujol and A. Gourdon, *Chem. Rev.* **2017**, *117*, 1407-1444.

[17] C. Bohne, *Chem. Soc. Rev.* **2014**, *43*, 4037-4050.

[18] a) O. I. Wilner and I. Willner, *Chem. Rev.* **2012**, *112*, 2528-2556; b) M. Madsen and K. V. Gothelf, *Chem. Rev.* **2019**, *119*, 6384-6458; c) A. V. Pinheiro, D. Han, W. M. Shih and H. Yan, *Nat. Nanotechnol.* **2011**, *6*, 763-772; d) K. V. Gothelf, *MRS Bull.* **2017**, *42*, 897-903; e) T. Torring, N. V. Voigt, J. Nangreave, H. Yan and K. V. Gothelf, *Chem. Soc. Rev.* **2011**, *40*, 5636-5646; f) K. V. Gothelf and T. H. LaBean, *Org. Biomol. Chem.* **2005**, *3*, 4023-4037; g) X. Wang, A. R. Chandrasekaran, Z. Shen,

Y. P. Ohayon, T. Wang, M. E. Kizer, R. Sha, C. Mao, H. Yan, X. Zhang, S. Liao, B. Ding, B. Chakraborty, N. Jonoska, D. Niu, H. Gu, J. Chao, X. Gao, Y. Li, T. Ciengshin and N. C. Seeman, *Chem. Rev.* **2019**, *119*, 6273-6289; h) P. Wang, G. Chatterjee, H. Yan, T. H. La Bean, A. J. Turberfield, C. E. Castro, G. Seelig and Y. Ke, *MRS Bull.* **2017**, *42*, 889-896; i) F. Hong, F. Zhang, Y. Liu and H. Yan, *Chem. Rev.* **2017**, *117*, 12584-12640; j) Y. Hu and C. M. Niemeyer, *Adv. Mater.* **2019**, *31*, 1806294; k) B. Saccà and C. M. Niemeyer, *Angew. Chem. Int. Ed.* **2012**, *51*, 58-66; l) U. Feldkamp and C. M. Niemeyer, *Angew. Chem. Int. Ed.* **2006**, *45*, 1856-1876.

[19] F. De Leo, A. Magistrato and D. Bonifazi, *Chem. Soc. Rev.* **2015**, *44*, 6916-6953.

[20] a) H. Qiu, J. C. Dewan and N. C. Seeman, *J. Mol. Biol.* **1997**, *267*, 881-898; b) E. Winfree, F. Liu, L. A. Wenzler and N. C. Seeman, *Nature* **1998**, *394*, 539-544; c) S. Pitchiaya and Y. Krishnan, *Chem. Soc. Rev.* **2006**, *35*, 1111-1121; d) H. Li, J. D. Carter and T. H. LaBean, *Mater. Today* **2009**, *12*, 24-32; e) M. R. Jones, N. C. Seeman and C. A. Mirkin, *Science* **2015**, *347*, 1260901; f) Q. Hu, H. Li, L. Wang, H. Gu and C. Fan, *Chem. Rev.* **2019**, *119*, 6459-6506; g) H. Zuo and C. Mao, *Adv. Drug Deliv. Rev.* **2019**, *doi.org/10.1016/j.addr.2019.02.002*.

[21] N. C. Seeman, *J. Theor. Biol.* **1982**, *99*, 237-247.

[22] J. Malo, J. C. Mitchell, C. Vénien-Bryan, J. R. Harris, H. Wille, D. J. Sherratt and A. J. Turberfield, *Angew. Chem. Int. Ed.* **2005**, *44*, 3057-3061.

[23] N. R. Kallenbach, R.-I. Ma and N. C. Seeman, *Nature* **1983**, *305*, 829-831.

[24] a) R. I. Ma, N. R. Kallenbach, R. D. Sheardy, M. L. Petrillo and N. C. Seeman, *Nucleic Acids Res.* **1986**, *14*, 9745-9753; b) M. L. Petrillo, C. J. Newton, R. P. Cunningham, R.-I. Ma, N. R. Kallenbach and N. C. Seeman, *Biopolymers* **1988**, *27*, 1337-1352.

[25] a) Y. Wang, J. E. Mueller, B. Kemper and N. C. Seeman, *Biochemistry* **1991**, *30*, 5667-5674; b) X. Wang and N. C. Seeman, *J. Am. Chem. Soc.* **2007**, *129*, 8169-8176.

[26] J. Sharma, Y. Liu and H. Yan in *Structural DNA nanotechnology: Information guided self-assembly*, World Scientific, **2011**, pp. 65-84.

[27] T. H. LaBean, H. Yan, J. Kopatsch, F. Liu, E. Winfree, J. H. Reif and N. C. Seeman, *J. Am. Chem. Soc.* **2000**, *122*, 1848-1860.

[28] P. W. K. Rothemund, *Nature* **2006**, *440*, 297-302.

[29] N. C. Seeman, F. Liu, C. Mao, X. Yang, L. A. Wenzler, R. Sha, W. Sun, Z. Shen, X. Li, J. Qi, Y. Zhang, T.-J. Fu, J. Chen and E. Winfree, *J. Biomol. Struct. Dyn.* **2000**, *17*, 253-262.

[30] N. C. Seeman, *Biochemistry* **2003**, *42*, 7259-7269.

[31] Y. Liu, Y. Ke and H. Yan, *J. Am. Chem. Soc.* **2005**, *127*, 17140-17141.

[32] H. Yan, S. H. Park, G. Finkelstein, J. H. Reif and T. H. LaBean, *Science* **2003**, *301*, 1882-1884.

[33] S. H. Park, P. Yin, Y. Liu, J. H. Reif, T. H. LaBean and H. Yan, *Nano Letters* **2005**, *5*, 729-733.

[34] A. Holmberg, A. Blomstergren, O. Nord, M. Lukacs, J. Lundeberg and M. Uhlén, *Electrophoresis* **2005**, *26*, 501-510.

[35] J. Zhang, Y. Liu, Y. Ke and H. Yan, *Nano Letters* **2006**, *6*, 248-251.

[36] Y. He, Y. Chen, H. Liu, A. E. Ribbe and C. Mao, *J. Am. Chem. Soc.* **2005**, *127*, 12202-12203.

[37] C. Zhang, M. Su, Y. He, X. Zhao, P.-a. Fang, A. E. Ribbe, W. Jiang and C. Mao, *Proc. Natl. Acad. Sci.* **2008**, *105*, 10665-10669.

[38] Y. He, Y. Tian, A. E. Ribbe and C. Mao, *J. Am. Chem. Soc.* **2006**, *128*, 15978-15979.

[39] U. Majumder, A. Rangnekar, K. V. Gothelf, J. H. Reif and T. H. LaBean, *J. Am. Chem. Soc.* **2011**, *133*, 3843-3845.

[40] Y. He, Y. Tian, Y. Chen, Z. Deng, A. E. Ribbe and C. Mao, *Angew. Chem. Int. Ed.* **2005**, *44*, 6694-6696.

[41] X. Sun, S. Hyeon Ko, C. Zhang, A. E. Ribbe and C. Mao, *J. Am. Chem. Soc.* **2009**, *131*, 13248-13249.

[42] F. Zhang, Y. Liu and H. Yan, *J. Am. Chem. Soc.* **2013**, *135*, 7458-7461.

[43] D. Chavey in *TILINGS BY REGULAR POLYGONS—II A CATALOG OF TILINGS*, (Ed. I. Hargittai), Pergamon, Amsterdam, **1989**, pp. 147-165.

[44] F. Zhang, S. Jiang, W. Li, A. Hunt, Y. Liu and H. Yan, *Angew. Chem. Int. Ed.* **2016**, *55*, 8860-8863.

[45] W. Liu, H. Zhong, R. Wang and N. C. Seeman, *Angew. Chem. Int. Ed.* **2011**, *50*, 264-267.

[46] Y. Suzuki, M. Endo and H. Sugiyama, Nat. Commun. 2015, 6, 8052.

[47] S. Woo and P. W. K. Rothemund, *Nat. Chem.* **2011**, *3*, 620.

[48] Y. Suzuki, H. Sugiyama and M. Endo, Angew. Chem. Int. Ed. 2018, 57, 7061-7065.

[49] P. Wang, S. Gaitanaros, S. Lee, M. Bathe, W. M. Shih and Y. Ke, *J. Am. Chem. Soc.* **2016**, *138*, 7733-7740.

[50] A. Gopinath and P. W. Rothemund, *ACS Nano* **2014**, *8*, 12030-12040.

[51] R. J. Kershner, L. D. Bozano, C. M. Micheel, A. M. Hung, A. R. Fornof, J. N. Cha, C. T. Rettner, M. Bersani, J. Frommer and P. W. Rothemund, *Nat. Nanotechnol.* **2009**, *4*, 557-561.

[52] A. Aghebat Rafat, T. Pirzer, M. B. Scheible, A. Kostina and F. C. Simmel, *Angew. Chem. Int. Ed.* **2014**, *53*, 7665-7668.

[53] S. Ramakrishnan, S. Subramaniam, A. F. Stewart, G. Grundmeier and A. Keller, *ACS Appl. Mater. Interfaces* **2016**, *8*, 31239-31247.

[54] S. Hamada and S. Murata, *Angew. Chem. Int. Ed.* **2009**, *48*, 6820-6823.

[55] C. Tian, C. Zhang, X. Li, C. Hao, S. Ye and C. Mao, *Langmuir* **2013**, *30*, 5859-5862.

[56] M. Li, H. Zuo, J. Yu, X. Zhao and C. Mao, *Nanoscale* **2017**, *9*, 10601-10605.

[57] H. Qian, J. Yu, P. Wang, Q.-F. Dong and C. Mao, *Chem. Commun.* **2012**, *48*, 12216-12218.

[58] Y. Ke, L. L. Ong, W. Sun, J. Song, M. Dong, W. M. Shih and P. Yin, *Nat. Chem.* **2014**, *6*, 994.

[59] Y. Ke, L. L. Ong, W. M. Shih and P. Yin, *Science* **2012**, *338*, 1177.

[60] a) Y. Yang and C. Wang, *Philos. Trans. Royal Soc. A* **2013**, *371*, 20120311; b) X. Ma, L. Liu, X. Mao, L. Niu, K. Deng, W. Wu, Y. Li, Y. Yang and C. Wang, *J. Mol. Biol.* **2009**, *388*, 894-901; c) X.-B. Mao, C.-X. Wang, X.-K. Wu, X.-J. Ma, L. Liu, L. Zhang, L. Niu, Y.-Y. Guo, D.-

H. Li, Y.-L. Yang and C. Wang, *Proc. Natl. Acad. Sci.* **2011**, *108*, 19605-19610; d) X. Mao, X. Ma, L. Liu, L. Niu, Y. Yang and C. Wang, *J. Struct. Biol.* **2009**, *167*, 209-215; e) N. Kalashnyk, J. T. Nielsen, E. H. Nielsen, T. Skrydstrup, D. E. Otzen, E. Lægsgaard, C. Wang, F. Besenbacher, N. C. Nielsen and T. R. Linderoth, *ACS Nano* **2012**, *6*, 6882-6889.

[61] a) L. Liu, L. Zhang, X. Mao, L. Niu, Y. Yang and C. Wang, *Nano Lett.* **2009**, *9*, 4066-4072; b) F. Qu, L. Yu, H. Xie, Y. Zheng, J. Xu, Y. Zou, Y. Yang and C. Wang, *J. Phys. Chem. C* **2017**, *121*, 10364-10369; c) Y. Yu, Y. Yang and C. Wang, *ChemPhysChem* **2015**, *16*, 2995-2999; d) L. Liu, L. Niu, M. Xu, Q. Han, H. Duan, M. Dong, F. Besenbacher, C. Wang and Y. Yang, *ACS Nano* **2014**, *8*, 9503-9510.

[62] a) L. Niu, L. Liu, W. Xi, Q. Han, Q. Li, Y. Yu, Q. Huang, F. Qu, M. Xu, Y. Li, H. Du, R. Yang, J. Cramer, K. V. Gothelf, M. Dong, F. Besenbacher, Q. Zeng, C. Wang, G. Wei and Y. Yang, *ACS Nano* **2016**, *10*, 4143-4153; b) L. Niu, L. Liu, M. Xu, J. Cramer, K. V. Gothelf, M. Dong, F. Besenbacher, Q. Zeng, Y. Yang and C. Wang, *Chem. Commun.* **2014**, *50*, 8923-8926.

[63] a) D. Marsh, *Biochem. J.* **1996**, *315*, 345-361; b) S. Sek, T. Laredo, J. R. Dutcher and J. Lipkowski, *J. Am. Chem. Soc.* **2009**, *131*, 6439-6444; c) P. Pieta, J. Mirza and J. Lipkowski, *Proc. Natl. Acad. Sci.* **2012**, *109*, 21223-21227.

[64] S. Abb, L. Harnau, R. Gutzler, S. Rauschenbach and K. Kern, *Nat. Commun.* **2016**, 7, 10335.

[65] U. Lewandowska, W. Zajaczkowski, S. Corra, J. Tanabe, R. Borrmann, E. M. Benetti, S. Stappert, K. Watanabe, N. A. K. Ochs, R. Schaeublin,

C. Li, E. Yashima, W. Pisula, K. Müllen and H. Wennemers, *Nat. Chem.* **2017**, *9*, 1068-1072.

[66] L. Schlipf, T. Oeckinghaus, K. Xu, D. B. R. Dasari, A. Zappe, F. F. de Oliveira, B. Kern, M. Azarkh, M. Drescher, M. Ternes, K. Kern, J. Wrachtrup and A. Finkler, *Sci. Adv.* **2017**, *3*, e1701116.

[67] a) D. Moll, C. Huber, B. Schlegel, D. Pum, U. B. Sleytr and M. Sára, *Proc. Natl. Acad. Sci.* **2002**, *99*, 14646-14651; b) I. Reviakine and A. Brisson, *Langmuir* **2001**, *17*, 8293-8299.

[68] a) R. A. McMillan, C. D. Paavola, J. Howard, S. L. Chan, N. J. Zaluzec and J. D. Trent, *Nat. Mater.* **2002**, *1*, 247-252; b) S. R. Hall, W. Shenton, H. Engelhardt and S. Mann, *ChemPhysChem* **2001**, *2*, 184-186; c) U. B. Sleytr, P. Messner, D. Pum and M. Sára, *Angew. Chem. Int. Ed.* **1999**, *38*, 1034-1054; d) U. B. Sleytr, E. M. Egelseer, N. Ilk, D. Pum and B. Schuster, *FEBS J.* **2007**, *274*, 323-334; e) S. Howorka, *J. Mater. Chem.* **2007**, *17*, 2049-2053.

[69] T. J. Beveridge, *Curr. Opin. Struct. Biol.* **1994**, *4*, 204-212.

[70] X. Mo, M. P. Krebs and S. M. Yu, *Small* **2006**, *2*, 526-529.

[71] B. Schuster, *Biosensors* **2018**, *8*, 40.

[72] a) M. J. Ellis, S. Knapp, P. J. B. Koeck, Z. Fakoor-Biniaz, R. Ladenstein and H. Hebert, *J. Struct. Biol.* **1998**, *123*, 30-36; b) P. J. B. Koeck, H. K. Kagawa, M. J. Ellis, H. Hebert and J. D. Trent, *Biochim. Biophys. Acta, Protein Struct. Mol. Enzymol.* **1998**, *1429*, 40-44.

[73] I. Yamashita, *Thin Solid Films* **2001**, *393*, 12-18.

[74] J. Zhang, K. Zhou, Y. Zhang, M. Du and Q. Wang, *Adv. Mater.* **2019**, 1901485.

[75] P. Ringler and G. E. Schulz, *Science* **2003**, *302*, 106-109.

[76] J. C. Sinclair, K. M. Davies, C. Vénien-Bryan and M. E. M. Noble, *Nat. Nanotechnol.* **2011**, *6*, 558-562.